Geodesy and Geodynamics 12 (2021) 65–92

Contents lists available at ScienceDirect

Geodesy and Geodynamics

journal homepage: http://www.keaipublishing.com/geog

Assessment of hybrid geoids in Chile and Spain, combining GGM and GNSS/Leveling observations

José Antonio Tarrío Mosquera [a, *], Marcelo Caverlotti Silva [a], Fernando Isla [a], Carlos Prado [b]

[a] University of Santiago of Chile (USACH), Faculty of Engineering, Geographical Engineering Department, Chile
[b] Geographic Military Institute, Chile

ARTICLE INFO

Article history:
Received 6 July 2020
Accepted 20 December 2020
Available online 6 March 2021

Keywords:
GNSS levelling
Correcting surface
IHRS
SIRGAS
EIGEN-6C4

ABSTRACT

This research presents the results for analyses done to five geopotential global models (GGM), comparing them with ground data from GNSS and leveling in heterogenic zones from the geodetic perspective, in Chile and Spain. While the official and complete implementation of the International Height Reference Frame (IHRF) has not yet been established, the vertical geodetic system of many countries is not calculated on a global scale; instead, it is calculated by the variation of relative heights between one or more local tide gauges, such as in the case of Spain and Chile. This aspect creates regional and specific altimetry data, which disables the use of GGM to directly obtain the orthometric height of the vertical reference system (VRS) from the GNSS heights. Global models currently reach centimetric precision due to their high resolution but are directly incompatible for a local level. To solve this, we expose in this article the contrast between geometric geoidal undulation (ellipsoidal heights and orthometric data from the leveling networks in Spain and Chile) with the geoidal undulation in more recent models and higher resolution: Earth Gravitational Model 2008 (EGM08), European Improved Gravity model of the Earth by New techniques (EIGEN6C4), Gravity Observation Combination (GOCO05C), Experimental Gravity Field Model (XGM2016), and Ultra-High Resolution Global Geopotential Model (SGG-UGM), adjusting the residual between both referential heights by different parametric models and polynomials of determined order. Once evaluated, their geoidal undulations are combined with GNSS/leveling data from the corresponding VRS to generate a correcting surface, which is also known as a hybrid geoid, resulting in a model of optimal adjustment for the combination of five parameters of the EIGEN-6C4 with orthometric heights and ellipsoids of both Chile and Spain. The results show 2–3 cm precisions, which were statistically analyzed to determine the suitability for use. The final products are three grids of independent hybrid geoids, one for northern Spain and two for Chile (central and north), which allow continuous access to the VRS of each country using the GNSS's full potential until the IHRF is available and ready for use.

1. Introduction

In July 2015, in the city of Prague (Czech Republic), at the International Union of Geodesy and Geophysics (IUGG), International Association of Geodesy (IAG), resolution number one resolved five conventions for the International Height Reference System (IHRS), where it is clearly explained that the vertical coordinates shall be potential differences between the reference potential $W_0 = (62636853.4\ m^2/s^2)$[1], and the potential W_P of the Earth's gravity field at the points designated P. The potential differential $-\Delta W_P$ shall be designated as a geopotential number $C_P = -\Delta W_P = W_0\text{-}W_P$. Although there are indeed efforts to implement the IHRS

* Corresponding author.
E-mail addresses: jose.tarrio@usach.cl, centro.usc@usach.cl (J.A. Tarrío Mosquera).

Peer review under responsibility of Institute of Seismology, China Earthquake Administration.

Production and Hosting by Elsevier on behalf of KeAi

https://doi.org/10.1016/j.geog.2020.12.003

globally, there is still local vertical datum, for example, in Spain and Chile. The purpose of this study is to use the potential of the Global Navigation Satellite System (GNSS) measurements in two completely different zones from the geodetic perspective, one with frequent earthquakes such as Chile and another with rare seismic events such as Spain, to be able to access local "physical" heights temporarily until the IHRS is formally established.

Until that time, on a regional level, Gauss's famous equation that combines ellipsoidal (h), orthometric (H), and geoidal undulation (N) heights, $H = h\text{-}N$, should not be correct, complicating the use of GNSS systems to obtain orthometric heights directly on the physical heights networks, something that will not happen with the IHRS. In an initial approach, the fundamental relation that links the heights measured over the ellipsoidal and geoidal surfaces related to the vertical geodetic datum, which is established generally from gravity and/or leveling data, is defined by [2]:

$$h - H - N = 0 \tag{0.1}$$

where h is the ellipsoidal height above the ellipsoid, measured by the length of the normal of itself and that obtained through GNSS observations, H is the orthometric height measured on the normal to the geoid and obtained from the vertical network datum, and N is the geoidal undulation, which can be obtained from a regional gravimetric geoidal model or Geopotential Global Models (GGM). Currently, equation (0.1) is not wholly valid due to different systematics linked to one or many components of the equation: different parameters of the ellipsoid, different hypotheses to calculate the orthometric height, different tide systems for H and N, different time and reductions, etc. The most common terms for typical deviation are the ones gives by the geoidal undulation [3] having the ellipsoidal and orthometric height with a precision 10 times better than N; this translates into mm in the case of h and H, cm for N, and therefore cm for the combination of heights [4].

In contrast, the advantage of the GGM is that it possesses a greater quantity of data because of its global orbits of the Earth, obtaining in this way access to undulations in further points of the leveling lines. The residuals generated in equation (0.1) can be modeled. It is necessary to analyze each component of error, evaluating the residuals so that when they are modeled, they can predict the physical height at any point in the field of study [5], being able to combine the continuity of the GGM with the local precision of the vertical reference system (VRS) and the access to the Global Reference Frame with the GNSS data of the ellipsoidal heights.

The objective of this study is to "join" ellipsoidal (h), orthometric (H), and geoidal undulation (N) heights of the GGMs to generate a corrected surface that is compatible with all heights in a continuous way. From the orthometric heights, from which materialize the vertical reference system (SRV) of each country; the ellipsoidal heights, in Spain referred to as European Reference Frame(EUREF) and in Chile as Geocentric Reference System for the Americas(SIRGAS); and the geoidal undulations coming from the GGM continuous access to the local VRS will be generated by modeling the residuals coming from the combination of the three heights.

To make this determination, a combination of heights is calculated to integrate the height of the GNSS and the coverage of the GGMs with the official altimetry of the country; this creates what is called a "corrective surface" or hybrid geoid [6]. There are different types of modeling and surfaces to correct the residuals [7]. In this study we used models of similarity of four, five and seven parameters, with four and five being generally used [3]. We also employ a first-order polynomial (1×1) and another of third order (3×3) with the idea to explore the verisimilitude of the hybrid geoid found. In this paper, the problem is explored and analyzed, evaluating two completely different environments from the geophysical point of view, one of them with a completely dynamic frame of reference (Chile) and another almost static (Spain) [8].

For the selection of the GGM, we have reviewed the state of the art of the most recent models and those with higher resolution [9]. The chosen models were the following: Earth Gravitational Model 2008 (EGM08) [10], European Improved Gravity model of the Earth by New techniques (EIGEN-6C4) [11], Gravity Observation Combination (GOCO05C) [12], and Ultra-High Resolution Global Geopotential Model (SGG-UGM-1). It is worth noting that only a few of them have been analyzed and compared to the designated zones, for example, GOCO03S in Argentina [13,14] and above all in Brazil [15], and EIGEN-6C4 in Chile [16] with the differences among the different heights at a decimetric order. In the case of Spain, an evaluation has been done with the EGM08 by the National Geographic Institute of Spain (IGN), presenting differences of the scale of 56.1 cm and typical deviations of 50 mm [17], where different results are also produced if they are compared to other available studies [18,19].

2. Methodology. Hybrid geoid modeling

In modeling the combination of data from different heights, it is vital to reconcile epochs and tidal systems. The first challenge is to ensure that all data are consistent along time, and the second is to ensure that the GNSS data, orthometric heights, and GGM undulations are in the same system.

The current and previous International Terrestrial Reference Frame (ITRF) [20], is densified in Latin America and Europe through SIRGAS and EUREF respectively. Therefore, to homogenize the epochs of ellipsoidal heights, there are two velocity models, Velocity Model for SIRGAS (VEMOS) [21] and EUREF Velocity Model [22]. Since the VEMOS model only represents horizontal velocities, for h we use velocities from non-lineal models, following the instructions in [23] and calculated at the USC Geodetic Analysis and Processing Center [24]. The epoch change for the Chilean data was made from a surface deformation model generated from the 10-year time series (2010–2020) of data from free access stations in Chile [25], processed with Bernese 5.2 software [26] and interpolating the solution with spline interpolation, and modeling of the residuals. Since it is a confidential project currently in progress [27], the information cannot be expanded. It is shown on the map in Fig. 1. Related to the data in Spain, EUREF velocities were used at the closest stations to reconcile the epoch, as in the case of stations ACOR00ESP and VIGO00ESP, both belonging to EUREF [28].

In Spain, the change in height due to the epoch is approximately 2 mm per year for ACOR and 0.9 mm for VIGO. This means that the ellipsoidal height will have a minimal change in its h component. The orthometric height remains in epoch 2008.

For Chile, the problem is of greater complexity. For the orthometric height of central Chile, the study started analyzing the displacement produced by the Maule 2010 earthquake. We initially used the authors' work for the central leveling line [29], but the results were unsatisfactory. Our theory is that they used the wrong epoch for the definition of the height H. When performing validation with new geometric leveling data, it was observed that it was not possible to change the orthometric epoch with this previously presented model. What we did do was to separate two epochs, one for one tide gauge and another for another, 2019 and 2017, based on the new leveling data. In the north we kept the epoch of orthometric height.

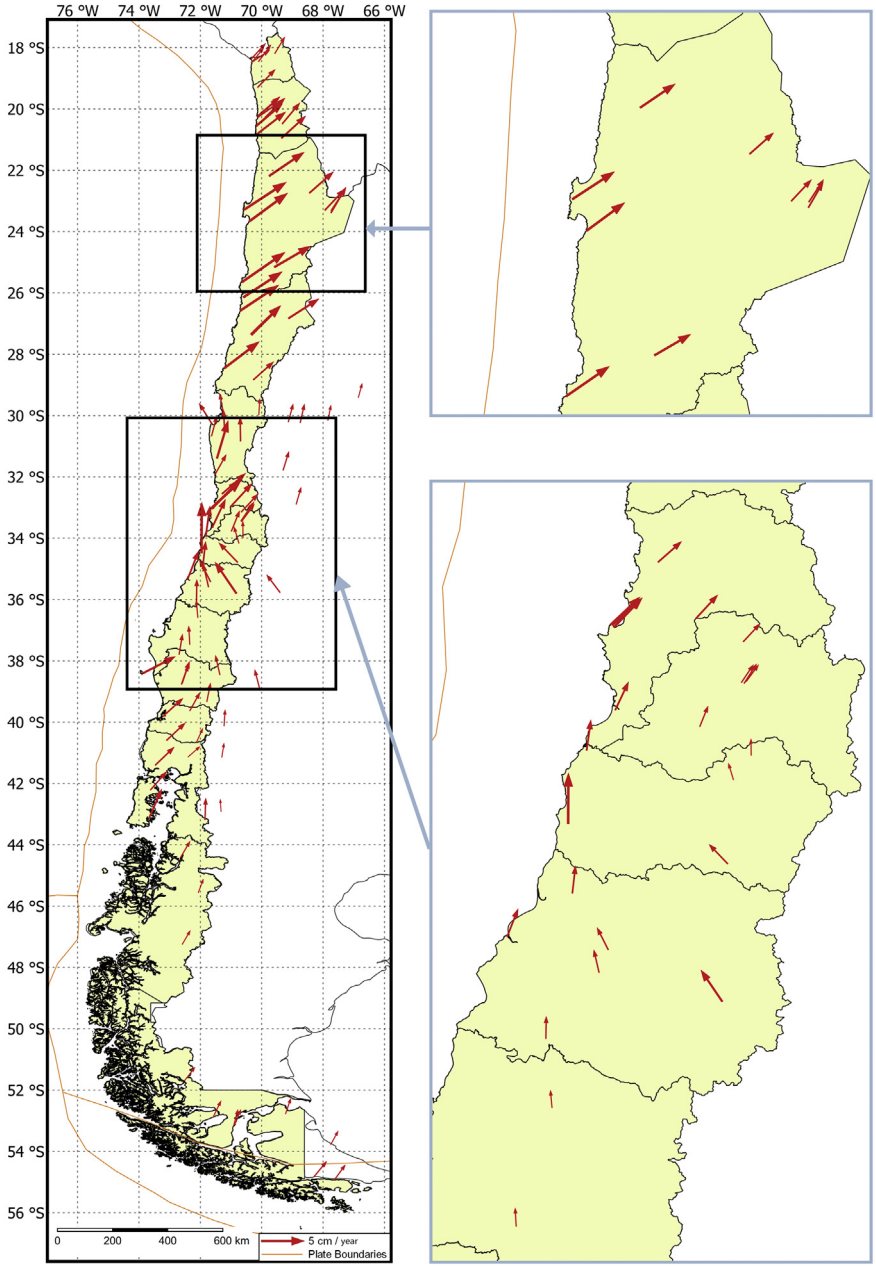

Fig. 1. Displacement vectors used to model the epoch in Chile.

Concerning the ellipsoidal height, we directly use our models because the previous study [29] has a period from 2007 to 2015, which is insufficient in space and time for compatibility the ellipsoidal height's epoch. It is crucial to indicate that the change in ellipsoidal height ranges oscillates from 30 mm to 120 mm approximately for the central zone. The fiducial points were always SIRGAS stations.

As a summary, the initial epochs of the data are shown in Table 1.

We reconciled the epoch of the GNSS data with the VRS data, leaving the orthometric height as an inherent systemic within the model. As will be discussed below, this worked perfectly in the northern zone of Chile. However, some errors were perceived at the center of Chile in some determined zones that the model could not perform appropriately due to the different epochs. The final epochs compatibilized to perform the adjustment are shown in the Table 2.

The importance of the epoch's harmonizing shows in Fig. 2 for the 5 parameters (5P) model on EGM08 in central Chile. On the left are the residuals without homogenizing epochs, and on the right are the same residuals homogenizing the epochs. We can see the residuals' magnitude, which is almost 40 cm without harmonizing, while with the correct epoch, it reaches a maximum of 6 cm. In Spain, the change is inconsequential because the epoch's changes

Table 1
Initial epoch for three height types.

	h	H	N
North Chile	2019 and 2014	2014	GGM epoch
Central Chile	2019,2017,2014,2012	2019,2017,2012, 2006,2002	
Spain	2010,2008	2008	

Table 2
Final epoch for three height types.

	h	H	N
North Chile	2019	2014	GGM epoch
Central Chile	2019	2019,2017	
Spain	2010	2008	

do not exceed 4 mm. This highlights the importance of epoch's homogenization.

The other aspect of consideration is the tidal system, which has to be the same in the three heights. The ellipsoidal heights at the benchmarks obtained from fiducial points of SIRGAS and EUREF depend hierarchically on the ITRF, which is calculated in a tide-free system. Therefore, the data of the VRS from Chile and Spain (orthometric heights), which are calculated on a mean sea level, are converted from a mean sea to a tidal-free system according to [30], to be compatible with the reference frame data from Spain and Chile, with the equation:

$$H^{TF} = H^{MF} - 0.68 \times \left(0.099 - 0.296\ \sin^2 \varphi\right) \tag{1.1}$$

where φ is the geodetic latitude observed at the benchmark and H^{MT} is the orthometric height of the SRV at each country.

Now we only need the GGM data, which in order to be consistent with h y H were obtained on a tidal-free system directly from the International Centre for Global Earth Models (ICGEM), with the only change in the C_{20} coefficient of the spherical harmonics in the representation of geopotential.

Once the input data (h, H, and N) were compatible, we performed the combination. For this, the geoid undulation obtained from GGM, which will be denoted N^{GGM}, and calculated by using geometric data $N^{GNSS/Niv}$, must comply with the following expression:

$$h_i - H_i - N_i^{GGM} = 0 \tag{1.2}$$

$$N_i^{GNSS/Niv} - N_i^{GGM} = 0 \tag{1.3}$$

Another approach is to deal with the problem from a relative perspective.

$$\Delta h_i - \Delta H_i - \Delta N_i^{GGM} = 0 \tag{1.4}$$

The system can be expressed in an absolute or relative way, that is, with relative height increments $(\Delta h, \Delta H, \Delta N)$. In this study, we use absolute heights and not relatives, due to the lack of complete cofactor matrices of the respective calculations of VRS in Chile and Spain. However, the relative increments were used to analyze and later eliminate gross errors at verifying the $\Delta h_i, \Delta H_i, \Delta N_i^{MGG}$ at consecutive points whose value is greater than 3σ, since the tendency at these points should be the same [31].

There are many practical reasons why equation (1.2) does not comply, because the residuals must be analyzed and modeled. Although many of the reasons are described in [3], the principal ones are these:

- Data for the three heights refer to different reference surfaces.
  - h: refers to the reference ellipsoid used to determine the orbits of satellites.
  - H: refers to the local vertical datum, defined by the fixation of one or more tidal gauge stations.
  - N: refers to the reference surface used in the global geopotential model that cannot be the same as the anomalies in gravity.
- There is instability at the passive reference monuments, through the passing of time.
- There are systematic effects and distortions, mainly caused by geoidal mistakes of long-wave longitude. These mistakes can be noted on gravimetric geoidal models due to the differences between data sources related to the reference system they adopt, and they also are contained in the ellipsoidal heights, such as for example atmospheric refraction, that produce measurements not adequately on GNSS.

To model the residuals that are produced by the sources previously mentioned, we use here what is named “hybrid geoids,” “geometric geoids,” or “correcting surface,” combining data from satellite missions to obtain a continuous undulation, with GNSS/leveling data obtaining a discrete undulation over the leveling grid from GNSS observations over leveling benchmarks [7,32]. The calculation is done by including a correction factor to the data in order to comply with equation (1.2):

$$h - N - c = H + \tilde{v} \tag{1.5}$$

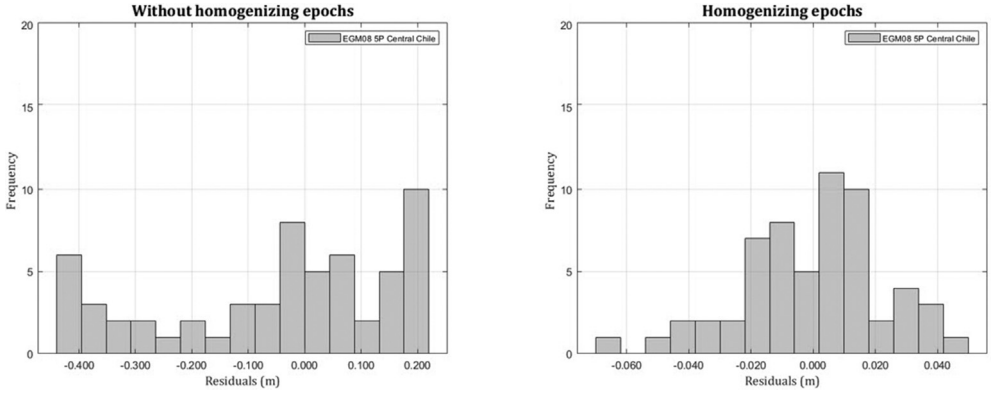

Fig. 2. Residual histograms without/with epoch homogenization.

where c represents the terms of the correction surface and $\tilde{v}$ represents aleatory errors. Due to the data redundancy, it can be denoted for each point:

$$\underbrace{\boldsymbol{h_i} - \boldsymbol{H_i} - \boldsymbol{N_i}}_{\boldsymbol{l_i}} = \boldsymbol{a_i^T x} + \tilde{\boldsymbol{v}}_{\boldsymbol{i}} \tag{1.6}$$

$$\underbrace{\underbrace{(\boldsymbol{h_i} - \boldsymbol{H_i})}_{\boldsymbol{N^{SRV}}} - \boldsymbol{N^{GGM}}}_{\boldsymbol{l_i}} = \boldsymbol{a_i^T x} + \tilde{\boldsymbol{v}}_{\boldsymbol{i}} \tag{1.7}$$

2.1. Adjustment

Using matrix notation to solve the system, the functional model would be [33,34]:

$$\boldsymbol{l} = \boldsymbol{Ax} + \tilde{\boldsymbol{v}} \tag{1.8}$$

where the initial hypothesis for the stochastic model is:

$$E(\tilde{\boldsymbol{v}}) = 0; \tilde{\boldsymbol{v}} \sim N(0, \sigma_{\tilde{v}}{}^2 \boldsymbol{CV}_{\tilde{\boldsymbol{v}}}) \tag{1.9}$$

Here $\boldsymbol{l}_{\boldsymbol{mx1}}$ is the observation matrix (height misclosure); $\boldsymbol{A}_{\boldsymbol{mxu}}$ the design matrix, which depends on the parametric model used; $\boldsymbol{x}_{\boldsymbol{ux1}}$ the unknown parameter vector and $\tilde{\boldsymbol{v}}_{\boldsymbol{mx1}}$ the residual term; being m the number of points obtained from $\boldsymbol{l_i} = \boldsymbol{h_i} - \boldsymbol{H_i} - \boldsymbol{N_i}$; and u the number of model parameters. Equation (1.8) will be solved by the least squares principle, because the system is redundant, minimizing the $\tilde{\boldsymbol{v}}_{\boldsymbol{i}}$ residual according to:

$$\tilde{\boldsymbol{v}}^{\mathbf{T}} \boldsymbol{P} \tilde{\boldsymbol{v}} = minimun \tag{1.10}$$

The $\hat{\boldsymbol{x}}$ system solution for the u parameters is:

$$\hat{\boldsymbol{x}} = \left(\boldsymbol{A}^{\mathbf{T}} \tilde{\boldsymbol{P}} \boldsymbol{A}\right)^{-1} \times \boldsymbol{A}^{\mathbf{T}} \tilde{\boldsymbol{P}} \boldsymbol{l} \tag{1.11}$$

And adjusted residuals $\hat{\tilde{\boldsymbol{v}}}$ is:

$$\hat{\tilde{\boldsymbol{v}}} = \boldsymbol{A}\hat{\boldsymbol{x}} - \boldsymbol{l} \tag{1.12}$$

Equation (1.11) represents the solution with the residuals $\tilde{\boldsymbol{v}}$ of the different heights together, but they can separate, as we will see in the following paragraphs. The residual term $\tilde{\boldsymbol{v}}_{\boldsymbol{mx1}}$ is composed for each of the height data types, as follows:

$$\tilde{\boldsymbol{v}} = \boldsymbol{v_h} - \boldsymbol{v_H} - \boldsymbol{v_N} \tag{1.13}$$

$\tilde{\boldsymbol{v}}_{\boldsymbol{mx1}}$ can be separated by component using matrix **B**, according to.

$$\tilde{\boldsymbol{v}} = \boldsymbol{Bv} \tag{1.14}$$

employing an $\boldsymbol{I}_{\boldsymbol{mxm}}$ unit matrix.

$$\boldsymbol{B} = [\boldsymbol{I} - \boldsymbol{I} - \boldsymbol{I}] \tag{1.15}$$

It is important to indicate that the residual term $\boldsymbol{v}$ is composed of:

$$\boldsymbol{v} = \begin{bmatrix} \boldsymbol{v_h} \\ \boldsymbol{v_H} \\ \boldsymbol{v_N} \end{bmatrix} \tag{1.16}$$

The $\boldsymbol{CV}$ matrix is:

$$E(\boldsymbol{v_h}) = 0; \boldsymbol{v_h} \sim N\left(0, \sigma_h^2 \boldsymbol{CV_h}\right) \tag{1.17}$$

$$E(\boldsymbol{v_H}) = 0; \boldsymbol{v_H} \sim N\left(0, \sigma_H^2 \boldsymbol{CV_H}\right) \tag{1.18}$$

$$E(\boldsymbol{v_N}) = 0; \boldsymbol{v_N} \sim N\left(0, \sigma_N^2 \boldsymbol{CV_N}\right) \tag{1.19}$$

Continuing with the separate least squares resolution, this is done by minimum squares according to the Gauss-Markov model [35], minimizing $\boldsymbol{v}$ according to:

$$\boldsymbol{v}^{\mathbf{T}} \boldsymbol{P} \boldsymbol{v} = \boldsymbol{v}_{\boldsymbol{h}}^{\mathbf{T}} \boldsymbol{P_h} \boldsymbol{v_h} + \boldsymbol{v}_{\boldsymbol{H}}^{\mathbf{T}} \boldsymbol{P_H} \boldsymbol{v_H} + \boldsymbol{v}_{\boldsymbol{N}}^{\mathbf{T}} \boldsymbol{P_N} \boldsymbol{v_N} = minimun \tag{1.20}$$

Here $\boldsymbol{P}$ is the weight matrix and $\boldsymbol{CV}$ is the variance-covariance matrix related by:

$$\boldsymbol{P}_{\boldsymbol{mxm}} = \begin{bmatrix} \boldsymbol{P_h} & 0 & 0 \\ 0 & \boldsymbol{P_H} & 0 \\ 0 & 0 & \boldsymbol{P_N} \end{bmatrix} = \begin{bmatrix} \boldsymbol{CV_h^{-1}} & 0 & 0 \\ 0 & \boldsymbol{CV_H^{-1}} & 0 \\ 0 & 0 & \boldsymbol{CV_H^{-1}} \end{bmatrix} \tag{1.21}$$

The system solution for the adjusted parameters u is:

$$\hat{\boldsymbol{x}} = \left(\boldsymbol{A}^{\mathbf{T}} (\boldsymbol{CV_h} + \boldsymbol{CV_H} + \boldsymbol{CV_N})^{-1} \boldsymbol{A}\right)^{-1} \times \boldsymbol{A}^{\mathbf{T}} (\boldsymbol{CV_h} + \boldsymbol{CV_H} + \boldsymbol{CV_N})^{-1} \boldsymbol{l} \tag{1.22}$$

Here $\boldsymbol{B}$ is the matrix that allows us to analyze the input of each residue, separating the $\boldsymbol{v}$ matrix as shown in equation 1.23:

$$\boldsymbol{B}\hat{\boldsymbol{v}} = \widehat{\boldsymbol{v_h}} + \widehat{\boldsymbol{v_H}} + \widehat{\boldsymbol{v_N}} \tag{1.23}$$

The fit of the separated residuals can be solved according to:

$$\hat{\boldsymbol{v}} = \boldsymbol{P}^{-1} \boldsymbol{B}^{\mathbf{T}} \left(\boldsymbol{B} \boldsymbol{P}^{-1} \boldsymbol{B}^{\mathbf{T}}\right) (\boldsymbol{l} + \boldsymbol{A}\hat{\boldsymbol{x}}) \tag{1.24}$$

and the residuals for each height adjusted would be:

$$\widehat{\boldsymbol{v_h}} = \boldsymbol{CV_h} (\boldsymbol{CV_h} + \boldsymbol{CV_H} + \boldsymbol{CV_N})^{-1} \boldsymbol{Ml} \tag{1.25}$$

$$\widehat{\boldsymbol{v_H}} = -\boldsymbol{CV_H} (\boldsymbol{CV_h} + \boldsymbol{CV_H} + \boldsymbol{CV_N})^{-1} \boldsymbol{Ml} \tag{1.26}$$

$$\widehat{\boldsymbol{v_N}} = -\boldsymbol{CV_N} (\boldsymbol{CV_h} + \boldsymbol{CV_H} + \boldsymbol{CV_N})^{-1} \boldsymbol{Ml} \tag{1.27}$$

and the $\boldsymbol{M}$ matrix is:

$$\mathbf{M} = \boldsymbol{I} - \boldsymbol{A}\left(\boldsymbol{A}^{\mathbf{T}} (\boldsymbol{CV_h} + \boldsymbol{CV_H} + \boldsymbol{CV_N})^{-1} \boldsymbol{A}\right)^{-1} \boldsymbol{A}^{\mathbf{T}} (\boldsymbol{CV_h} + \boldsymbol{CV_H} + \boldsymbol{CV_N})^{-1} \tag{1.28}$$

With the two options explained, residuals joined or separated, as in equations (1.24–1.27), respectively, we have to decide which one to use. Our decision is to fit with residuals together due to the lack of separate $\boldsymbol{CV}$ matrices in the input data, using equation (1.11) and leaving (1.22) for future studies where we have the complete $\boldsymbol{CV}$ matrices.

The complete study of the hybrid geoid modeling was based on two goals, first solving and evaluating the $\boldsymbol{x}$ term, which includes refining and calculating the values that minimize $\tilde{\boldsymbol{v}}$, and secondly, to conveniently analyze the residuals in the final solution [36]. Since we do not have the $\boldsymbol{CV_h}, \boldsymbol{CV_H}, \boldsymbol{CV_N}$ matrices of the adjustments in all the lines of the VRS leveling calculation networks that are generated by the different geographic institutes, but we do know the absolute values of the residuals from the initial data h, H,

y N, the option is to simplify the equation system by substituting the term $(\boldsymbol{CV_h} + \boldsymbol{CV_H} + \boldsymbol{CV_N})^{-1}$ from a typically combined deviation, from:

$$\tilde{\boldsymbol{P}} = \frac{1}{\sigma_h^2} + \frac{1}{\sigma_H^2} + \frac{1}{\sigma_N^2} \tag{1.29}$$

This may be a controversial aspect of the study, but we prefer to take a conservative perspective on it.

2.2. Study models

As we saw, the equation system 1.8 is solved by the least square method, adjusting according to the Gauss-Markov model for every GGM evaluated, paying special attention to the model used to minimize systematic effects and data inconsistencies. The design of the $\boldsymbol{A}$ matrix depends on the parametric model used to model the residue, here employing three similarity models of seven, five, and four parameters [2]:

$$f_{7P}(\varphi,\lambda) = x_1\cos\varphi\cos\lambda + x_2\cos\varphi\sin\lambda + x_3\sin\varphi + x_4\frac{\sin\varphi\cos\varphi\sin\lambda}{k} + x_5\frac{\sin\varphi\cos\varphi\cos\lambda}{k} + x_6\frac{1-f^2\sin^2\varphi}{k} + x_7\frac{\sin^2\varphi}{k} \tag{1.30}$$

In this case, k is $\sqrt{1-e^2\sin^2\varphi}$, e^2 the eccentricity and f the ellipsoid flattening, up to models of four and five parameters like in [33]:

$$f_{4P}(\varphi,\lambda) = x_0 + x_1\cos\varphi\cos\lambda + x_2\cos\varphi\sin\lambda + x_3\sin\varphi \tag{1.31}$$

$$f_{5P}(\varphi,\lambda) = x_0 + x_1\cos\varphi\cos\lambda + x_2\cos\varphi\sin\lambda + x_3\sin\varphi + x_4\sin^2\varphi \tag{1.32}$$

And two polynomials of first degree and third degree:

$$f_{1x1}(\varphi,\lambda) = x_0 + x_1(\lambda) + x_2(\varphi) \tag{1.33}$$

$$f_{3x3}(\varphi,\lambda) = x_0 + x_1(\lambda) + x_2(\varphi) + x_3(\lambda)^2 + x_4(\varphi)(\lambda) + x_5(\varphi)^2 + x_6(\lambda)^3 + x_7(\lambda)^2(\varphi) + x_8(\lambda)(\varphi)^2 + x_9(\varphi)^3 \tag{1.34}$$

The values of φ_i and λ_i represent the geodetic latitude and longitude observed through the VRS leveling benchmarks in EUREF or SIRGAS, according to the area. In the case of 7 parameters (7P), 5P, and 4 parameters (4P), the coefficient x_0 represents the displacement between N_i^{GGM} and $N_i^{GNSS/Niv}$, while the coefficients $x_{1\ldots7}$ are transformation parameters between GGM and GNSS/leveling data, which absorb the inconsistencies of the different height types. For the first- and third-degree polynomials, the coefficients only imply a greater degree of the surface for modeling the residuals, from a 1×1 plane to a warped 3×3 surface.

The complete form of the $\boldsymbol{A(mxu)}$ matrix is, for example, for the case of five parameters:

$$\boldsymbol{A}_{m\times5} = \begin{pmatrix} 1 & \cos\varphi_1\cos\lambda_1 & \cos\varphi_1\sin\lambda_1 & \sin\varphi_1 & \sin^2\varphi_1 \\ \vdots & \vdots & \vdots & \vdots & \vdots \\ 1 & \cos\varphi_m\cos\lambda_m & \cos\varphi_m\sin\lambda_m & \sin\varphi_m & \sin^2\varphi_m \end{pmatrix} \tag{1.35}$$

It is important to indicate here that an over-parameterization can lead to unrealistic results in places with gaps in leveling data or far from them, as we can see in Fig. 3.

where the $\boldsymbol{l}$ values have been modeled with a function of 5×5 parameters, obtaining an unreal surface when moving away from the modeling area. These unrealistic results, the product of mathematical adaptation, jeopardize the final purpose of the reference surface by not creating a truthful physical representation of the modeling residuals, but instead, an optimal mathematic adjustment that does not represent in the best way the surface of the GMM adapted to the corresponding VRS. This is a serious problem because a low root mean square (RMS) indicates a mathematically correct model, but it may be geodesically unreal. In order to avoid this, it is important to use cross-validation of data [3].

2.3. Model evaluation

After eliminating the mistakes, generally proceeding from the leveling lines or GNSS observations, which are used to model the parametric model, we proceed to evaluate the goodness of fit, being one of the most common methods, evaluate the statistics and the residue vectors after performing the least square adjustment according:

$$\hat{\boldsymbol{v}}_i = \boldsymbol{h_i} - \boldsymbol{H_i} - \boldsymbol{N_i^{GGM}} - \boldsymbol{A_i^T x} \tag{1.36}$$

A priori, the model with the lowest root mean square error or standard deviation (RMSE) of the residue vector will be the best adjustment model, but in order to avoid unreal surfaces, cross-validation will be done afterward. This offers a more realistic analysis by predicting the orthometric height at points aside from the calculation of the hybrid geoid. This process can be resumed in five steps [33,36]:

1. Select all the points of study but one.
2. Of the selected group, the combined adjustment must be applied by calculating the $\boldsymbol{x}$ parameters of the model.
3. Use the calculated model to predict the residual value of the point that was left out.
4. Compare the estimated values with the known height error for said point.
5. Repeat steps 1 to 4 for every reference point in the network and calculate the RMSE.

The RMSE value of cross-validation gives a more realistic indication of the accuracy of the selected model as a prediction surface for a new point, by making the cross-validation from one point to the other.

A procedure also evaluated to see the goodness of fit is the determination coefficient, denoted by R^2, which describes the ratio in which the square sums vary due to the adjustment:

$$R^2 = 1 - \frac{\sum_{i=1}^{m}\left(\boldsymbol{l_i} - \hat{\boldsymbol{v}}_i\right)^2}{\sum_{i=1}^{m}\left(\boldsymbol{l_i} - \bar{\boldsymbol{l}}_i\right)^2} \tag{1.37}$$

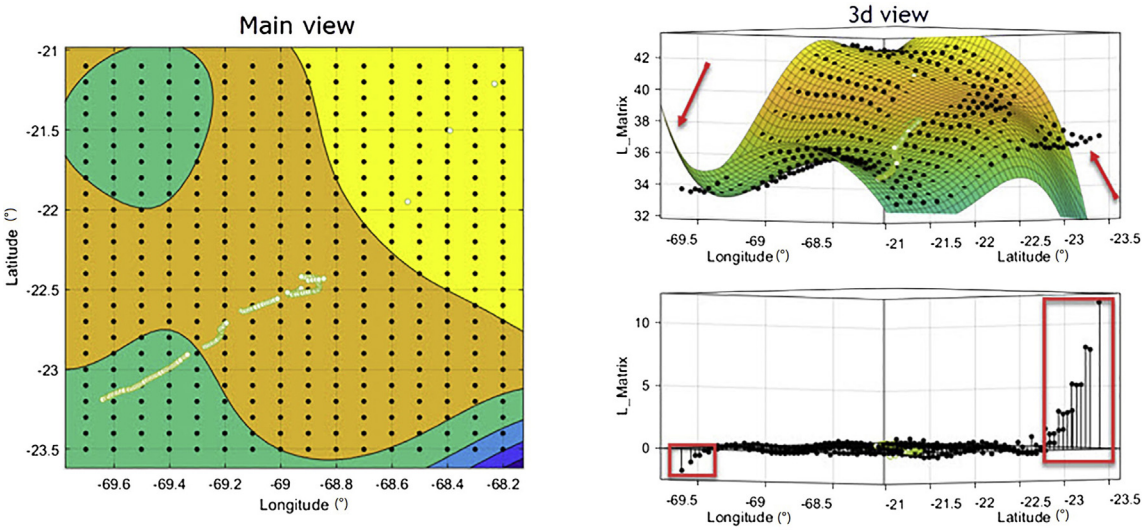

Fig. 3. Effects of the overuse of parameters. L values in meters.

where m is the number of observations and $\bar{\boldsymbol{l}}_{\boldsymbol{i}}$, the observations mean, where the perfect adjustment would be where $R^2 = 1$. Aside from R^2, the determination coefficient of the adjustment R_α^2 is also established, from which we obtain:

$$R_\alpha^2 = 1 - \frac{(m-1)}{(m-u)}\left(1 - R^2\right) \tag{1.38}$$

m is the number of observations and u the number of parameters. R_α^2 shows the ratio of the square sums due to the adjustment. R_α^2 may take any value less than or equal to 1, with a value closer to 1 the one that shows a better adjustment. Negative values may occur when the model has terms that do not help predict an answer. It is important to be careful about the values of R^2 and R_α^2 because if the degrees of freedom are small, we can obtain greater values independently of the validity of the adjustment; in cases such as these, a meticulous approach would be to perform a cross-validation data.

Generally, a $\sum_{i=1}^{m} (\boldsymbol{l}_{\boldsymbol{i}} - \widehat{\boldsymbol{v}}_{\boldsymbol{i}})^2$ is denoted as sum of squares due to error (SSE), where a value closer to 0 indicates that the model has a smaller random error component and that the adjustment will be more useful for the prediction; and $\sum_{i=1}^{m} (\boldsymbol{l}_{\boldsymbol{i}} - \bar{\boldsymbol{l}}_{\boldsymbol{i}})^2$ is denoted as total sum of squares (SST). Lastly, the root mean square error RMSE is defined as:

$$RMSE = \sqrt{\frac{\sum_{i=1}^{m}\left(\boldsymbol{l}_{\boldsymbol{i}} - \widehat{\boldsymbol{v}}_{\boldsymbol{i}}\right)^2}{m-u}} \tag{1.39}$$

$m-u$ are denoted (DoF degree of freedom). The statistics R^2, R_α^2, y RMSE will show the goodness of fit, along with the GGM and the model of choice.

3. Data used

At the end of the 1990s, the combination of height data from Global Positioning System (GPS) receivers combined with GGM acquired specific relevance thanks to the generation of the Earth Gravitational Model 1996 (EGM96) [37]. This geopotential model gives whole-Earth complete harmonic spherical coefficients for degree and order 360 [37], unseen for the period but insufficient for the actual requirements, from the geodesic level to the engineering level and large-scale cartography.

The roads toward a unified modern vertical system are well developed in Spain, as in the European Vertical Reference System (EVRS) [38], and in parts of Chile, through the VRS for SIRGAS [39,40]. In the future it is expected to be entirely unified with the adoption of the conventions from the International Height Reference System (IHRS) [41].

In Chile, the VRS is geometric and not physical, which means it was done basically with first-order leveling from the mean height of a determined tide gauge and some gravimetric measurements in distinct zones of the country, materializing leveling lines and international connections necessary to link Chile to Argentina and Bolivia. However, there is no global adjustment on a country-size level due to Chile's orography, something that does not happen with the VRS of Spain due to more available access to the country's boundaries. This is due to the fact that land connections in Spain are better than in Chile.

In the following part, the entry data for this study will be shown, to a local scale for the orthometric height (H) from VRS from Chile and Spain and to a global scale with the GMM's undulation (N) and the GNSS observations. The GNSS ellipsoidal height (h) observed over the SRV's benchmarks was processed with commercial software, Trimble Business Center (TBC) v. 4.0, using observable GPS and GLONASS constellations (Global'naya Navigatsionnaya Sputnikovaya Sistema).

3.1. Geodetic vertical network of Chile

The actual Vertical Reference Frame of Chile, as in many countries in South America and even the world, is still an old system, which means that according to [42]:

- The leveling reference is acquired by one or many tidal gauges over a period.
- The leveling was performed by geometric leveling, but the gravity (which could correct the unevenness) is not known in all points.
- The reference frame is static concerning the time.
- It is wrongly assumed that the geoid coincides with the mean sea level.

The calculation of the sea level along Chile is performed by the Chilean Navy Hydrographic and Oceanographic Service (SHOA),

through a series of tidal gauges along the coast. Then, the Geographic Military Institute (IGM) begins the geometric leveling along the territory, materializing the SRV from these local references.

Taking all the information available from the IGM [43] adds the problem that the geographic configuration of Chile has around 4200 km of coast. Also, a maximum width of 445 km in the northern zone makes it harder to use a single tidal gauge as a vertical reference, due to the fact that leveling from north to south must be much larger than from west to east, as is currently done. The Chilean VRS starts with all the geodesic measurements in altimetry in Chile, beginning in 1929, performing leveling lines from sea to mountain and starting from the tidal gauge in Cartagena (φ:-33.538427, λ:-71.6334441).

Due to Chile's geography as a narrow and elongated country, some links to other tidal gauges were established to refer to the leveling lines over time. Of the 86 tidal gauges available by the SHOA, IGM has used the tidal gauges which existed in the 1950s: those of Antofagasta, Valparaiso, Talcahuano, Puerto Montt, and Punta Arenas.

With the later addition of one in Arica for the international link with Bolivia, this created six altimetry references for the Chilean vertical geodetic network, which makes it one of few countries with this many references. To cover the entire Chilean terrain with altimetry and have data access to the altimetry reference frame in Chile, there is a network of 5000 points located on the main networks of the country. This IGM refers the Chilean's SRV to the height at medium sea level (MSL)from a network of 86 tidal gauges calculated and maintained by SHOA distributed along the coast of Chile [44], as seen in Fig. 4.

All of the different altimetry helped in the past for the creation and densification of the height reference. However, today is a problem with the accuracy of GGM along the country and above all, with the VRS of Chile, since there is no homogeneity and a high jump occurs concerning GGM. Chile is a long country, and access to benchmarks for the altimetry control is complicated. However, countries with similar coastal length have adopted at maximum two vertical datum points, such as the case of Argentina [45], located in the city of Mar del Plata and another in the city of Ushuaia, which will undoubtedly mitigate the change to the IHRS. In this study, we clarify the differences between VRS to the geopotential value W_0 of the GGM. One example of the differences is shown in Fig. 5.

There is a maximum difference of 67 cm between sea level registered by the tidal gauge in the city of Punta Arenas (Latitude: 53° 09′ 17.39″S, Longitude: 70° 54′ 40.64″ W) and that in the city of Arica (Latitude: 18° 28′ 28.56″ S, Longitude: 70° 17′ 52.51″ W), compromising in a certain way a future reconciliation between the potential W_0 with the local W_{local}. This aspect will be of great importance in the following sections since it is the fundamental reason to generate two hybrid geoid models, rather than one that covers the northern and southern zone of Chile in a single hybrid model. However, it undoubtedly can be implemented with the global physical heights once the IHRS arrives with homogeneity in heights.

A practically similar problem occurred on Australia, where the Australian Height Datum (AHD) referred to 30 tidal gauges along the Australian coast [47] and the Australian geoid 2020 “AusGeoid2020” [48], but that still does not manage to reconcile physical and geometrical heights. For this, a “corrective surface” is used, which resolves in Australia with the Australian Vertical Working Surface (AVWS) [4], with satisfactory results.

To analyze this variability in Chile, we have chosen two zones: one in the north of the country (more than 40% of Chile's GDP is

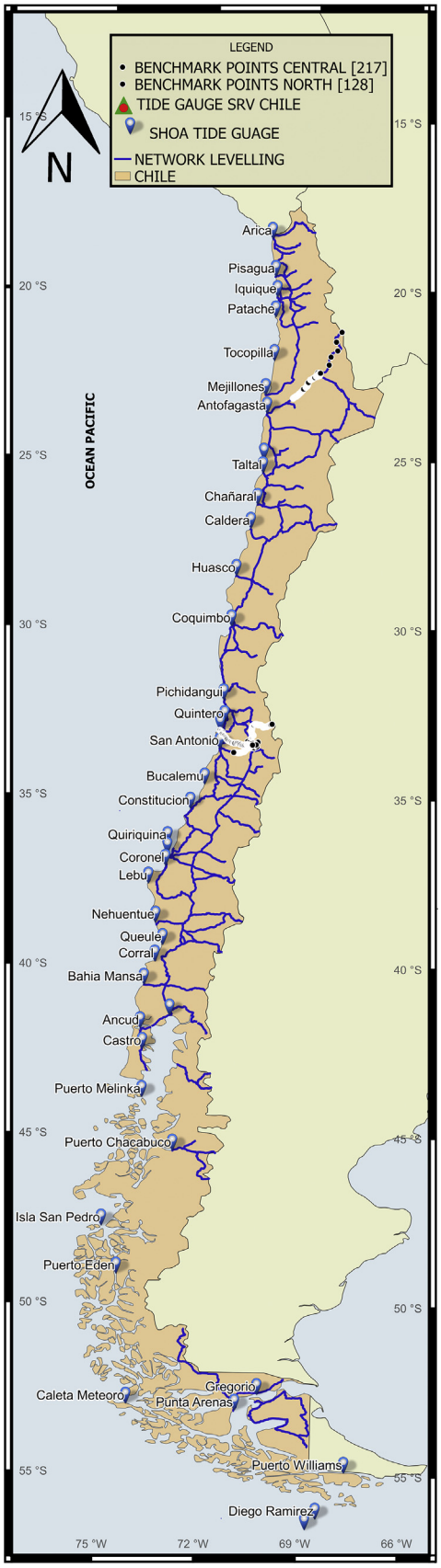

Fig. 4. SHOA tidal gauges.

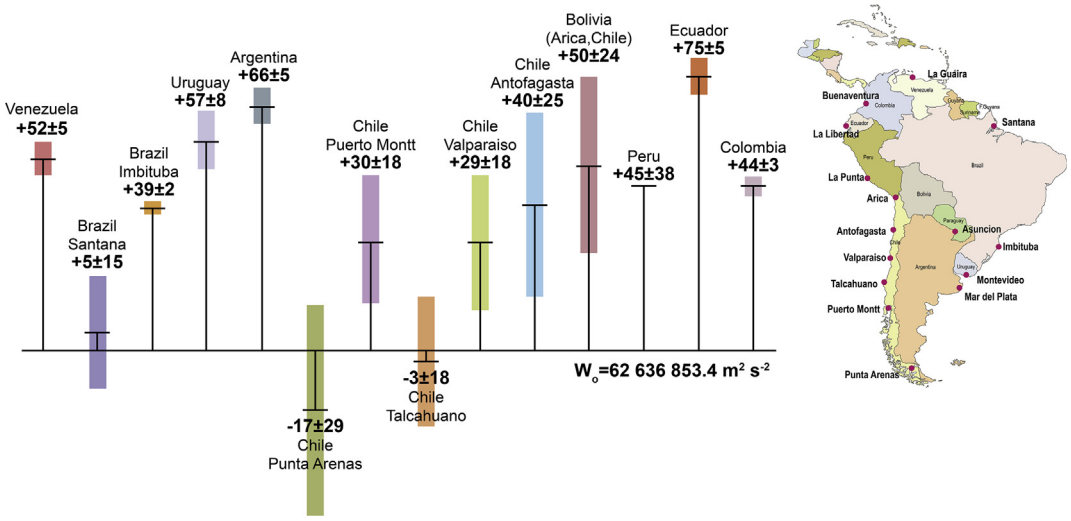

Fig. 5. Differences between local datum and W0. Source: [46].

there) and another in the more populated central zone, where the capital (Santiago de Chile) is located.

We will use two leveling lines from the sea to the Andes Mountain. The first location, which begins in Valparaiso and reaches the border with Argentina at Paso de Sico (Latitude 23°51′0.97″S, Longitude 67°14′56.14″W) with an approximate length of 430 km, will denominate the northern zone, shown in Fig. 6.

And the leveling line that goes from the Valparaiso tidal gauge to the border with Argentina at Paso Caracoles (Latitude 32°50′42.09″S, Longitude 70° 3′51.98″W), with an approximate length of 230 km, will denominate the central zone, shown in Fig. 7.

These two leveling lines refer to a mean tide system, which must later be corrected for the orthometric height. The GNSS data and accuracy of the ellipsoidal heights over the benchmarks, calculated from the SIRGAS-CON network and processed by TBC commercial software, are shown in Table 3.

The orthometric heights have an unknown deviation, so we use a $\sigma = 0.005$ m a generic precision.

The spatial location of the lines concerning the tidal gauges is shown in Fig. 8.

3.2. Geodetic vertical network of Spain

In the case of peninsular Spain, the VRS materialized with the REDNAP (*high precision leveling network, Red de Nivelación de Alta Precision)* takes as reference the mean sea level obtained by the only tidal gauge, located in the city of Alicante (38°30′N 0°30′W) and referencing the Mediterranean Sea. Starting from this point, the adjustment to the network it is made within geopotential heights, being observed ellipsoidal heights, gravity and, orthometric heights. The difference between heights in the Mediterranean Sea and the Cantabrian Sea reaches up to 28 cm over approximately 900 km [17], and that again clarifies the differences between orthometric heights. The organization in charge of maintaining and creating the Spanish VRS is the Geographic National Institute (IGN). The traditional European altimetry reference systems, established from the corresponding high-precision leveling national networks, are referred to as local vertical datum. Like in Chile, this leads to numerous inconveniences since the countries use different reference levels for diverse seas and oceans—the Baltic Sea, Northern Sea, Mediterranean Sea, Black Sea, Atlantic Ocean—reaching differences of various decimeters among them. Also, not all zero levels refer to the same sea level, with a few differences at low tide (Ostende) and others at high tide (Amsterdam). Thus, three different altitudes are used and are shown in Fig. 9.

The new REDNAP began in 1999 and was finished in 2007 in the Spanish peninsula and a year later at the Balearic Islands. The peninsular REDNAP has an approximate longitude of 16,500 km, taking a single fundamental point (NP1) in Alicante and a geopotential value of 3,34142 u. g. p., which refers to the tidal gauge in the same city. All of the network adjustments at geopotential points refer to the same value as Alicante [49], and the errors increase as we move away from the initial point, as seen in Fig. 10.

The previous leveling lines are referred to a mean tide system, something that should be corrected later.

The selected zone for the study's realization was the leveling subnetwork of the northeastern part of the peninsula, in Galicia's autonomous community (Northwest zone). The justification for this is the continuation of previous work started by the primary author in the zone [18]. Fig. 11 shows the area selected in Spain for the study.

In Galicia (Spain's Northwest zone), there are 21 lines and three ramifications, adding to the group of approximately 1400 leveling benchmarks. This is points with orthometric measurements to compare with the ellipsoidal GNSS, but with lesser precision than this, around the 0.100 m on the 81% of the signals and worse in some case. As understood from the previous lines, this precision in height does not allow us to reach the final objective, which is to have ellipsoidal height with good precision. Because of this, we decided to observe sufficient points in REDNAP to cover the zone of study with millimetric precision in the best of cases, and centimetric precision in the worst. For this, we make an observation over one REDNAP benchmark every 10 km, approximately, from which we obtain a final count of 111 points. It must be mentioned that when viewing all the benchmarks photographically, it would be impossible to measure them all because there are GPS shadows in many locations; obviously, those points were not measured. This would also be useless work since we pretend to know these geodesic models' tendency for a good modelation.

Fig. 6. Data used for the northern zone.

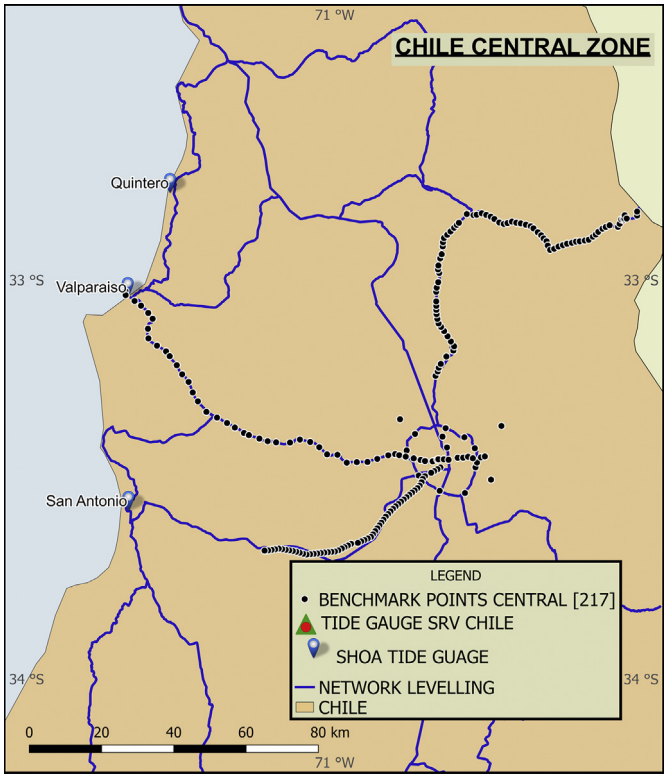

Fig. 7. Data used for the central zone.

Table 3
Summary of ellipsoidal height points in Chile.

	Area	No. of points	h_{MAX} (m)	h_{MIN} (m)	σ_{MAX}(m)	σ_{MIN} (m)
Central Zone	160 km × 120 km	217	3218.980	26.150	0.025	0.002
Northern Zone	270 km × 250 km	128	3922.303	1367.997	0.032	0.003

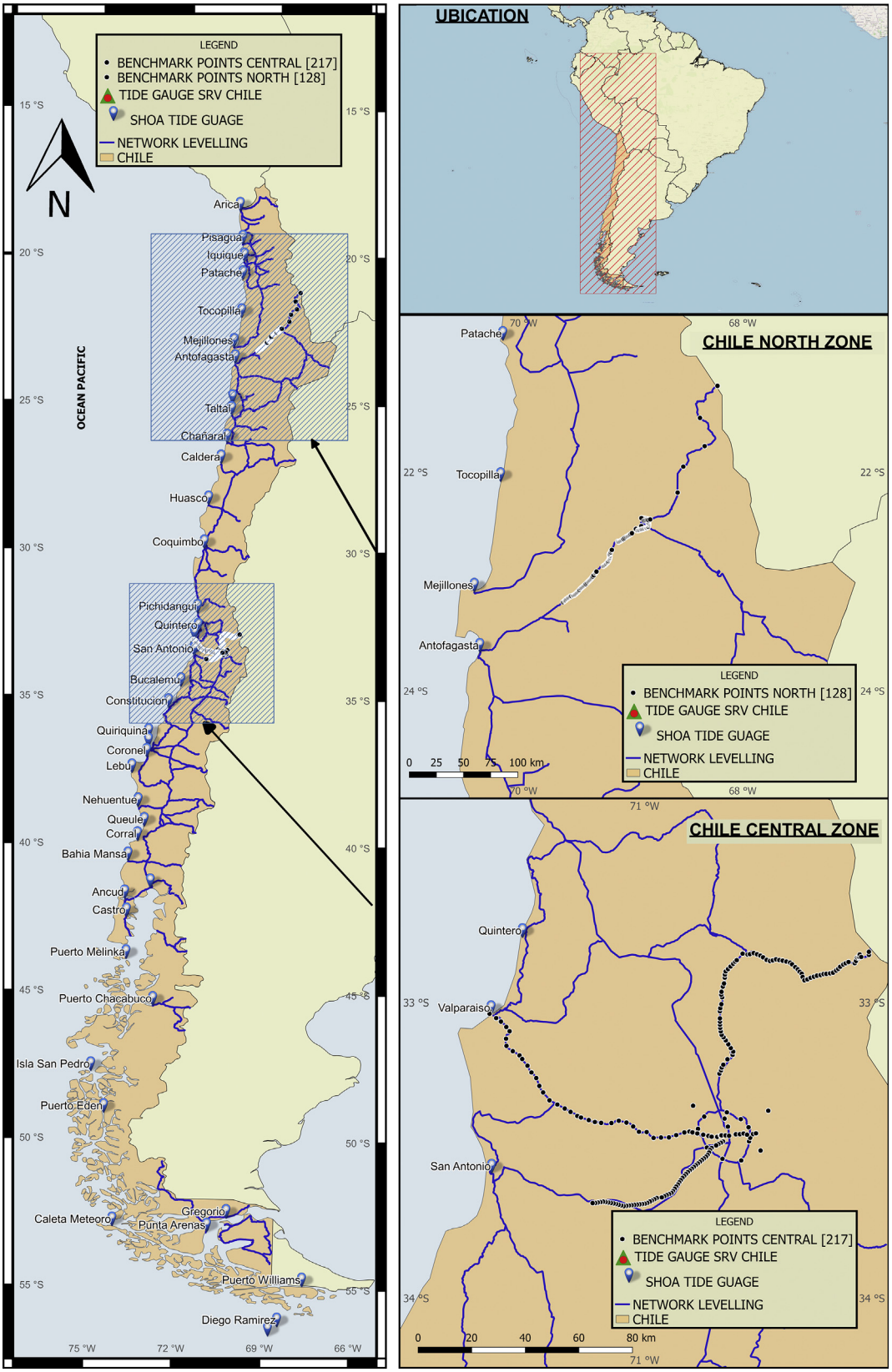

Fig. 8. VRS data for Chile used in the study.

The GNSS data and accuracy of the ellipsoidal heights over the benchmarks, calculated from the EUREF network, and processed with TBC commercial software, are the following, show in Table 4.

Regarding the orthometric heights, the adjustment precision of the points in the network is unknown. Although there are values on some nodes, this does not happen for others; for that reason, we decided to consider a generic precision for the benchmarks: $\sigma = 0.005$m.

3.3. Global geopotential models

When we talk about global geopotential models, we refer to a gravitational model of the Earth, whose function is to describe the gravity field (sum of gravitational attraction plus centrifugal force) in three dimensions. Above it has been generally calculated from different types of observations of the gravitational field, since long campaigns with direct measurements on the surface of the Earth, as well as gravimetric campaigns, vertical deflections, geopotential

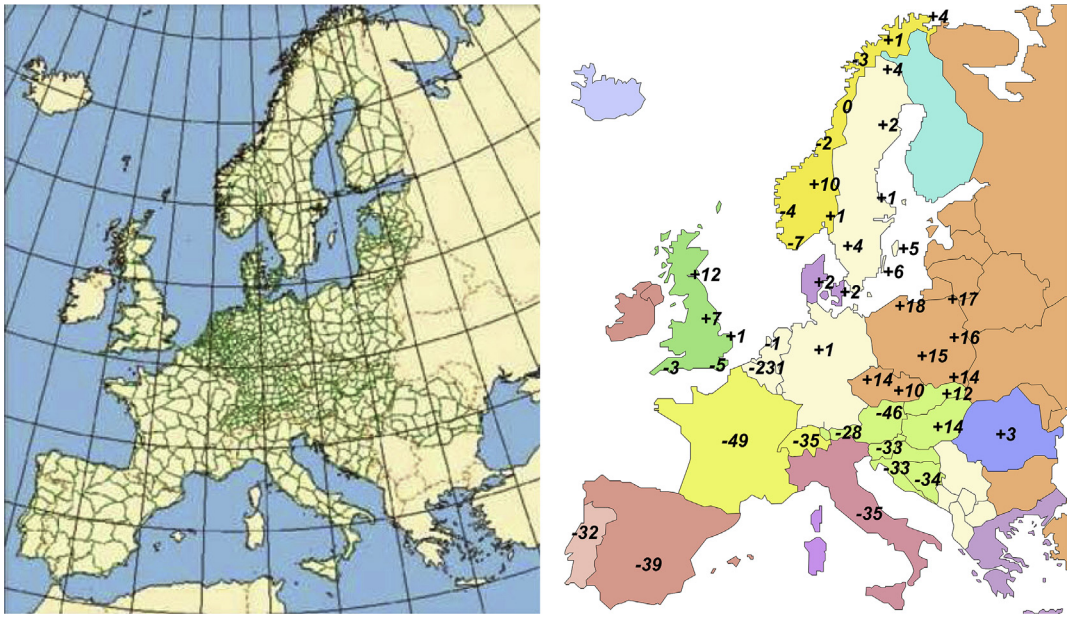

Fig. 9. State of the UELN 95/98 network in 2002 and differences between EUVN datum and different national datum. Source: [38].

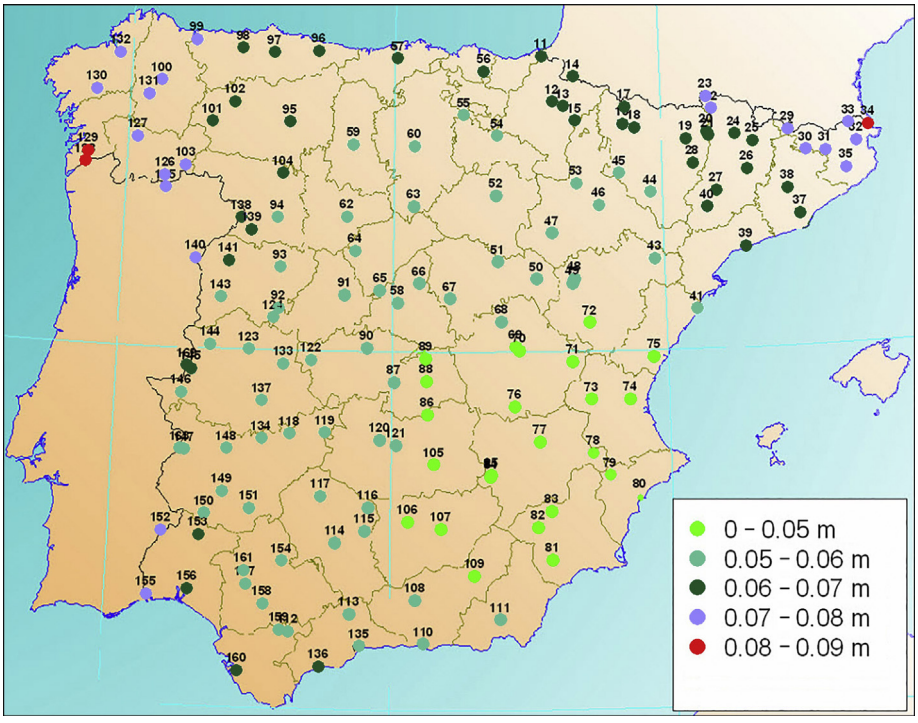

Fig. 10. REDNAP vector error. Source: [17].

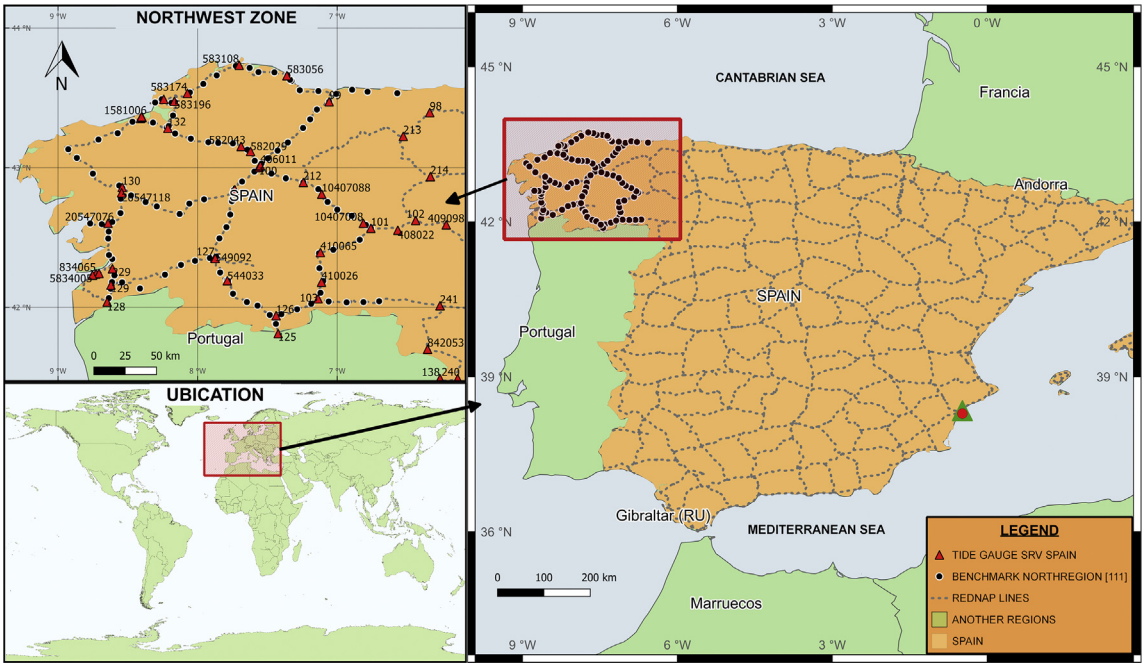

Fig. 11. Spanish vertical reference system.

Table 4
Summary of ellipsoidal heights points in Spain.

	Area	No. points	h_{MAX} (m)	h_{MIN} (m)	σ_{MAX} (m)	σ_{MIN} (m)
Northwest Zone	290 km × 250 km	111	1336.875	56.988	0.015	0.002

numbers, until the recent measurements of the gravity field on satellites such as CHAllenging Minisatellite Payload (CHAMP), Gravity Recovery and Climate Experiment (GRACE) or Gravity field and steady-state Ocean Circulation Explorer (GOCE) [50], representing the potential in harmonic spherical series. The function of the potential is expressed as the sum, to a certain determined degree and order, according to the following harmonic spherical expression:

$$V(r,\lambda,\varphi)=\frac{GM}{r}\sum_{l=0}^{l_{max}}\sum_{m=0}^{l}\left(\frac{R}{r}\right)^{l}P_{nm}(\sin\varphi)(C_{nm}\cos m\lambda+S_{nm}\sin m\lambda) \tag{2.1}$$

Here the values are as follows:

- r,λ,φ spherical coordinates of the evaluation point (radio, longitude, and latitude)
- R equatorial radius
- GM geocentric gravitational constant
- C_{nm},S_{nm} potential coefficients, which are determined from observations and depend on the distribution of the inner Earth masses
  - n evaluation on latitude
  - m evaluation on longitude
  - $n,m\lambda>0;n\geq m$
- $P_{nm(\cos\varphi)}$ Legendre functions, which define the behavior of the harmonic function ($m=0\rightarrow$ Legendre Polynomials)

The potential is known as the so-called equipotential surfaces, which are those imaginary surfaces in which the potential has the same value. One of the most important equipotential surfaces is the geoid, which is defined as the surface that coincides with the undisturbed marine surface (in other words, the sea in static equilibrium) and its fictional continuation below the continents. Geoids usually are the reference surface of a natural physical height; in other words, vertical datum. The correct choice of the geoid's surface in space must be based on the correct value of W_0 potentia [51]:

$$W(P)=W_0=\text{constant} \tag{2.2}$$

On an international level, the International Centre for Global Earth Models (ICGEM) [9] recovers and archives all of the GMM on its website, http://icgem.gfz-potsdam.de/home, from which the most recent and higher degrees are chosen for the study, according to Table 5.

The Earth Gravitational Model 2008 (EGM2008) is a model on spherical harmonics of the gravity potential of the Earth generated by the National Geospatial-Intelligence Agency (NGA) It is developed by a combination of a minimum square gravitational model ITG-GRACE03S and its covariance matrix, with gravity information obtained from a global group of anomalies of free-air gravity anomalies defined in a grid of 5′ arch. EGM2008 is complete to the degree and order 2159, and it contains additional coefficients up to the 2190 degree and 2159 order; its evaluation on zones of gravity density data goes from ±5 cm up to ±10 cm [52], compared with GPS/leveling data. EIGEN-6C4 is the fourth version of the European Improved Gravity model of the Earth by New techniques (EIGEN-6C series) and contains complete GGS data (Spaceborne Gravity Gradiometry) of the GOCE mission, its degree, and order on spherical harmonics is 2190. GPS/leveling

Table 5
Global geopotential models studied, and constituting the main source of data: follow-up data of satellite S, gravity data G, altimetry data A, GRACE, CHAMP, GOCE, LAser GEOdynamics Satellite (LAGEOS) Satellite Laser Ranging (SLR).

Model	Year	Data	Degree
EGM2008	2008	A, G, S(GRACE)	2190
EIGEN-6C4	2014	A, G, S(GOCE), S(GRACE), S(LAGEOS)	2190
SGG-UGM-1	2018	EGM2008, S(GOCE)	2159
EGM2008	2008	A, G, S(GRACE)	2190
GOCO-05c	2016	A, G, S(GRACE), S(GRACE)	720
XGM2016	2017	A, G, S(GOCO05s)	719

data evaluations show a standard deviation of 30.6 cm in South America and 20.9 cm in Europe [11]. The SGG-UGM-1 model developed by the School of Geodesy and Geomatics in Wuhan, China, is a model of ultra-high resolution, as shown in [53], of a degree and order 2159, developed with gravimetric data from EGM08. The model has been evaluated with GNSS/leveling data over China, the United States, and Brazil [54], with errors on the order of 74 cm in China, 32 cm in the United States, and 10 cm in Brazil. Lastly, we evaluated two more GGMs, GOCO05C (Gravity Observation Combination) [12] and the XGM2016 (Experimental Gravity Field Model), both developed by the Technical University of Munich (TUM). In the case of GOCO05, GRACE and GOCE data were employed, obtaining, as a result, a model of degree and order of 720, which has been evaluated with GPS/leveling data in Australia, Brazil, Germany, and the United States, with errors of 24, 31, 3.8, and 58 cm, respectively. XGM2016 is the result of the TUM evaluation of 15′x15 ′ grid data brought by the updated and revised NGA's gravity database, whose efforts are oriented toward the new Earth Gravity Model EGM2020. The GGM data interpolation on leveling points was obtained by a database of ICGEM, in a free tidal system, thus making it consistent with GNSS data and geometric leveling data of different VRS [55]. The relation of some of this GGM with W_0 can be reviewed in [1]. For the weight matrix of our modeling relative to the GGMs, we use each model's nominal precision.

4. Results and discussion

The initial undulation GGM values contrasting to local undulation without performing any type of adjustment are for the northeast of Spain, and the north and center of Chile, respectively:

In Tables 6–8 we observe that the undulation differences between the zones studied in Europe and South America are up to 25 m in some cases. Also, Fig. 12 graphically shows the different standard deviation, being the lowest in Spain and the highest in central Chile, and where the deviation of the values for northern and central Chile, in contrast with the VRS, is also greater than in Spain. It is important to note that in the initial data showed, we eliminate points with mistakes, generally coming from orthometric heights. This manifests itself when analyzing pairs of consecutive points through their relative differences.

From an absolute point of view, we can also observe that the VRS of Spain is closer to GGM's W_0 than the VRS of Chile, and the models with the lowest standard deviation are the ones of greater degree and order, in other words, EGM08 and EIGEN-6C4. This aspect does not happen in central Chile, due to the different tidal gauges used to materialize the SRV on the lines that reach

Table 6
Local and global initial undulations' statistics (m) in Spain.

Type of height	Maximum	Minimum	Range	Mean	Standard Deviation
N(GPS/leveling)	57.683	51.871	5.813	55.571	1.126
N EGM08	58.702	54.153	4.549	56.589	1.070
N EIGEN6C4	58.740	54.196	4.543	56.612	1.072
N GOCO05c	58.681	53.975	4.706	56.631	1.123
N SGG-UGM-1	58.730	54.126	4.604	56.607	1.091
N XGM2016	58.680	54.010	4.670	56.638	1.107

Table 7
Local and global initial undulations' statistics (m) in northern Chile.

Type of height	Maximum	Minimum	Range	Mean	Standard Deviation
N(GPS/leveling)	38.837	33.774	5.063	36.411	1.749
N EGM08	37.906	33.802	4.104	35.911	1.423
N EIGEN6C4	38.099	33.894	4.205	36.065	1.463
N GOCO05c	38.200	33.966	4.235	36.198	1.487
N SGG-UGM-1	38.081	33.916	4.165	36.080	1.440
N XGM2016	38.173	33.854	4.318	36.157	1.498

Table 8
Local and global initial undulations' statistics (m) in central Chile.

Type of height	Maximum	Minimum	Range	Mean	Standard Deviation
N(GPS/leveling)	34.062	21.743	12.320	27.717	2.780
N EGM08	33.631	21.867	11.764	27.657	2.669
N EIGEN6C4	33.397	22.127	11.270	27.911	2.504
N GOCO05c	33.055	21.994	11.061	27.804	2.571
N SGG-UGM-1	33.353	22.067	11.285	27.780	2.508
N XGM2016	33.139	22.006	11.134	27.990	2.567

Santiago de Chile. These differences may be because the expected precision of the models is from ±4 to ±6 cm in zones with data densification, while in zones with little densification it is from ±20 to ±40 cm [56], something possible because in the Andes this is small data terrain densification for these models. This aspect is not minor, since a transition in the local vertical datum to the IHRS will have a higher impact for the South American country than for the Iberian country, mainly because of Chile's different height references.

From Tables 6–8, we generate Table 9, which shows the relative differences between the global undulation and local undulation of the SRVs to analyze trends afterward.

In the case of Spain, the relative behavior of EGM08 and EIGEN-6C4 is practically similar to VRS, increasing the differences up to almost 5 cm for GOCO05C. This behavior is not seen in Chile, in the case of GOCO05C, clearly motivated by the difference of initial referential level and by the GGM resolution of the closest zones of the Andes Mountains, where the terrestrial data used for the creation were less.

For Chile's northern zone, this has more altitude above sea level, and the GGM standard deviation is closer to 30 cm in all cases. It is worth noting that we observed a bias of approximately 20 cm in the mean of the differences in EGM08, which is not present for the others, and currently, there is no information on the reason for this. It is worth noting that we observed a bias of approximately 20 cm in the mean of the differences in the case of EGM08, which is not present for the others; this also is unexplained. In central Chile, we observed a relative difference of 10 cm between EGM08 and GOCO

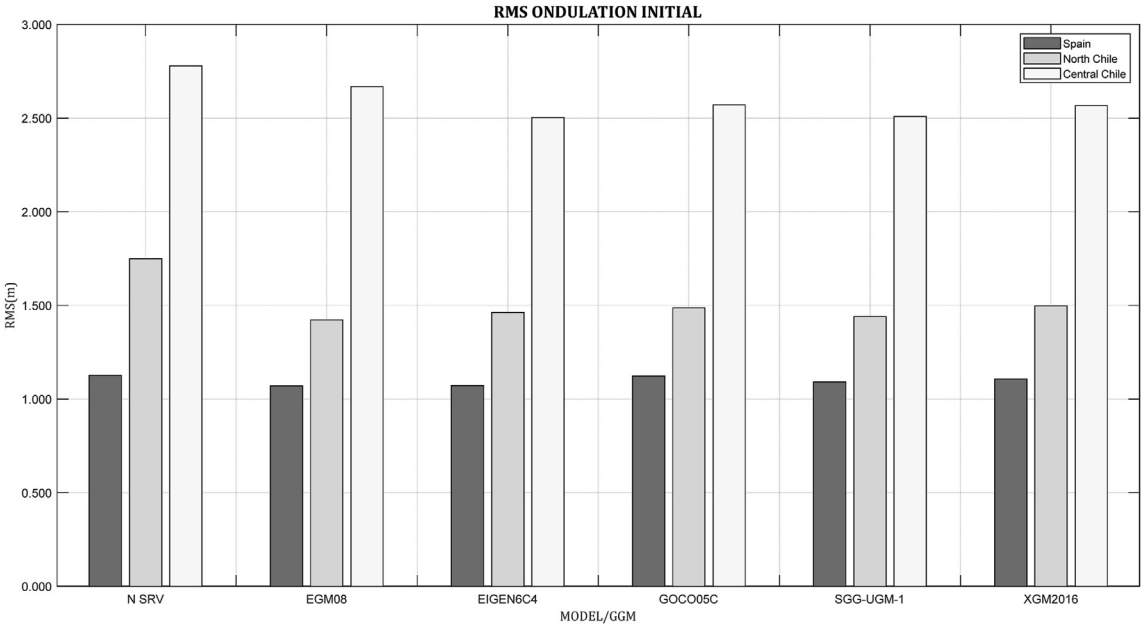

Fig. 12. RMS of GGM undulations by model.

05/XGM 2016; this difference increased to 17 cm for EIGEN-6C4 and SGG-UGM-1.

This initial analysis of Spain's hybrid geoid modeling already indicates that the better models of adjustment could be EGM08 and EIGEN-6C4. For Chile's case, in both the central and northern areas, this tendency has not been observed previously, since even though it is true that in the northern zone, EGM08 is practically the same as VRS, it does not happen to be the same in the central zone. This could be caused by the differences on the initial referential tidal gauge for both zones, which obviously is not the same as we saw previously with the Chilean Geodesic Vertical Network. In addition, it is worth mentioning that some GGMs have long-wave longitude problems on mountain terrain, especially in the Andes and the Himalayas. These problems were found by comparing the

Table 9
Initial comparative undulations of GGM and GNSS/leveling statistics, units in (m).

North Chile					
	Min	Max	Range	Mean	Std
$N^{EGM08} \_ N^{GNSS/Niv}$	−0.931	0.028	−0.959	−0.500	±0.325
$N^{EIGEN-6C4} \_ N^{GNSS/Niv}$	−0.738	0.120	−0.858	−0.346	±0.286
$N^{GOCO05C} \_ N^{GNSS/Niv}$	−0.637	0.192	−0.828	−0.213	±0.262
$N^{SGG-UGM-1} \_ N^{GNSS/Niv}$	−0.756	0.142	−0.898	−0.330	±0.309
$N^{XGM2016} \_ N^{GNSS/Niv}$	−0.664	0.080	−0.744	−0.254	±0.250
Central Chile					
	Min	Max	Range	Mean	Std
$N^{EGM08} \_ N^{GNSS/Niv}$	−0.350	0.163	−0.513	−0.007	±0.113
$N^{EIGEN-6C4} \_ N^{GNSS/Niv}$	−0.583	0.423	−1.007	0.252	±0.273
$N^{GOCO05C} \_ N^{GNSS/Niv}$	−0.926	0.290	−1.216	0.146	±0.201
$N^{SGG-UGM-1} \_ N^{GNSS/Niv}$	−0.628	0.363	−0.991	0.120	±0.270
$N^{XGM2016} \_ N^{GNSS/Niv}$	−0.841	0.302	−1.143	0.334	−0.202
North Spain					
	Min	Max	Range	Mean	Std
$N^{EGM08} \_ N^{GNSS/Niv}$	0.944	1.012	0.068	1.018	±0.001
$N^{EIGEN-6C4} \_ N^{GNSS/Niv}$	0.987	1.049	0.062	1.041	±0.003
$N^{GOCO05C} \_ N^{GNSS/Niv}$	0.766	0.990	0.224	1.060	±0.055
$N^{SGG-UGM-1} \_ N^{GNSS/Niv}$	0.917	1.040	0.122	1.036	±0.022
$N^{XGM2016} \_ N^{GNSS/Niv}$	0.801	0.990	0.189	1.067	±0.038

EGM2008 with gravity models that include GRACE and GOCE measurements [57]. Now, we proceed to model the residuals of equation (2.6), according to the chosen models 1 × 1, 3 × 3, 4P, 5P, and 7P.

4.1. Chile modeling

Because of the difference of altitude origin for the leveling network between Chile's northern and central zones, the analysis will first address an independent form.

4.1.1. Northern zone

The use of one of the mathematic models shown in Section 3 generates a group of five surfaces for each one of the GGMs. The calculations were carried out by modifying the curve-fitting tool in Matlab [58]. The initial adjustment had 128 points, which was reduced to 107 due to mistakes in the initial data. Some generated surfaces are shown in Fig. 13, wherein the upper part of the image, the generated surface, is observed to model the matrix $\boldsymbol{L}$'s residuals, and the lower part models the generated surface's residuals. The following modeled figures will have the same configuration.

In the previous images, in a completely visual manner, the heterogeneity of the surfaces can be observed to adapt to the same residuals. The surfaces, in the case of 3 × 3, form irregular figures with steep slopes out of the zone of study, which precludes any extrapolation.

The statistical results of the adjustment surfaces for each GGM and model are shown in Tables 10 and 11, Figs. 14 and 15 in an analytical and graphic form for northern and central Chile, respectively:

As seen in Table 10, the GGM that presents the best adjustment by the five models used is the EIGEN-6C4, with values close to 2.5 cm in models of greater degree; SGG-UGM-1 and XGM16 are those that have a practically error of 1.5 cm or more. We can also observe a better performance of GOCO05C over EGM08, which reaffirms those as mentioned above with absolute and relative values before performing the combination and modeling of heights. This same behavior can observe the coefficients R^2 and R^2_α, being a priori, the models with better adjustment the model 3 × 3 and 7P. This improvement of the new GGM over EGM08 is already evidenced in [59] over the VRS of Argentina.

Due to its better performance, in Fig. 16 we show the residual histograms for all modeling in the GGM EIGEN6C4.

Table 10
Statistics for the adjusted surface in the northern zone of Chile.

	SSE	R-Square	ADJ R-Square	RMSE(m)
EIGEN6C4				
5P	0.0942	0.9937	0.9935	0.028
3 × 3	0.0719	0.9952	0.9948	0.025
4P	0.1336	0.9911	0.9909	0.033
7P	0.0747	0.9950	0.9948	0.025
1 × 1	0.1349	0.9910	0.9909	0.033
EGM08				
5P	0.1026	0.9936	0.9934	0.029
3 × 3	0.0891	0.9945	0.9940	0.028
4P	0.2425	0.9849	0.9846	0.045
7P	0.0962	0.9940	0.9937	0.028
1 × 1	0.3094	0.9808	0.9805	0.050
SGG-UGM-1				
	SSE	R-Square	ADJ R-Square	RMSE(m)
5P	0.1091	0.9934	0.9932	0.030
3 × 3	0.0792	0.9952	0.9949	0.026
4P	0.2196	0.9868	0.9864	0.042
7P	0.0900	0.9946	0.9943	0.028
1 × 1	0.2214	0.9867	0.9864	0.042
GOCO 05C				
5P	0.1538	0.9872	0.9868	0.036
3 × 3	0.0823	0.9932	0.9926	0.027
4P	0.1705	0.9858	0.9855	0.038
7P	0.0852	0.9929	0.9926	0.027
1 × 1	0.2232	0.9815	0.9812	0.043
XGM16				
5P	0.2378	0.9793	0.9786	0.045
3 × 3	0.1309	0.9886	0.9877	0.034
4P	0.2945	0.9744	0.9738	0.049
7P	0.1426	0.9876	0.9870	0.035
1 × 1	0.3341	0.9710	0.9705	0.052

Analyzing the histograms and their distribution, the first-order polynomial (1 × 1) has a nominal precision of approximately 5 cm in all the GGMs and by all the models, but the error distribution is not normal. The above makes that Chilean geodesic normative like the Public Works Ministry [60] should consider these precisions and changed it the lineal models by similarity models.

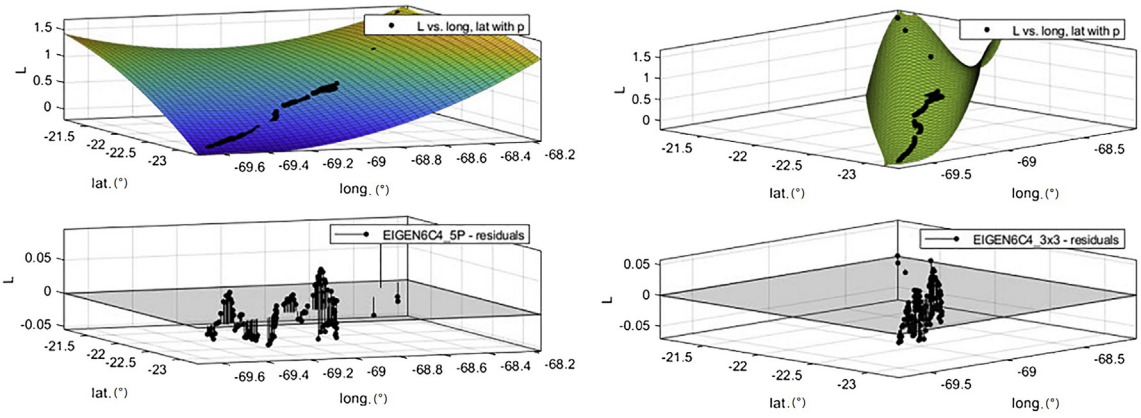

Fig. 13. 5P and 3 × 3 model over GGM EIGEN-6C4 northern zone.

Table 11
Adjusted surface statistics for the central zone of Chile.

	SSE	R-Square	ADJ R-Square	RMSE(m)
EIGEN6C4				
5P	0.0307	0.7758	0.7592	0.024
3 × 3	0.0199	0.8545	0.8278	0.020
4P	0.0552	0.5970	0.5751	0.032
7P	0.0259	0.8111	0.7893	0.022
1 × 1	0.1164	0.1499	0.1196	0.046
EGM08				
5P	0.0722	0.4953	0.4611	0.035
3 × 3	0.0374	0.7385	0.6949	0.026
4P	0.0745	0.4788	0.4528	0.035
7P	0.0546	0.6184	0.5782	0.031
1 × 1	0.0755	0.4721	0.4548	0.035
SGG-UGM-1				
3 × 3	0.0212	0.9039	0.8863	0.021
4P	0.0532	0.7595	0.7463	0.031
7P	0.0308	0.8608	0.8448	0.024
1 × 1	0.0712	0.6776	0.6661	0.036
5P	0.0425	0.8078	0.7935	0.028
GOCO 05C				
5P	0.0438	0.8850	0.8726	0.034
3 × 3	0.0108	0.9716	0.9635	0.018
4P	0.1548	0.5941	0.5621	0.064
7P	0.0433	0.8864	0.8670	0.035
1 × 1	0.1617	0.5759	0.5542	0.064
XGM16				
5P	0.0796	0.8976	0.8868	0.046
3 × 3	0.0287	0.9631	0.9531	0.029
4P	0.1579	0.7969	0.7813	0.064
7P	0.0697	0.9104	0.8955	0.044
1 × 1	0.2022	0.7399	0.7269	0.071

4.1.2. Central zone

The initial adjustment is done by starting with 217 points, which in the second adjustment goes to 120 points to perform the check, since it eliminates practically a complete line, which is the one that surrounds the city of Santiago de Chile. We believe this to be a mistake in the epoch. The IGM declares it to be from the year 2002, but when we check its realization's epoch with field data (epoch 2017) plus the earthquake jump, we can see a mistake in the informed epoch: there were more leveling epochs than indicated initially. In Fig. 17, we see the 5P and 3 × 3 models with the GGM EIGEN6C4, adjusted as seen in Section 2.1. The upper images show the correction surface, and the lower ones show the modeled residuals.

Both figures clearly show how the 3 × 3 model generates a more unrealistic surface to represent the residuals, away from benchmarks. The models are shown in Table 12 and graphs in Figs. 18 and 19.

In Chile's central zone, EIGEN-6C4 is the GGM that again performs better on general lines with precisions of the same order as the northern zone, around 2.5 cm on average for all models, with the worst adjustment for XGM16. Another clear result is the central zone's worse behavior in contrast to the northern zone, which is due to two aspects. There are two reference heights in the central zone, one that begins at the San Antonio tide gauge and another that begins at the Valparaíso tide gauge, where the zero reference height is not the same. The other differentiating aspect, with the most significant importance, is the proximity to one of the largest earthquakes in history (epicenter 35°54′32″S 72°43′59″W), which occurred on February 27, 2010, near the city of Concepción and which is located around 400 km from Santiago; in Santiago the earthquake displaced 22 cm of the VRS of the country.

Due to its better performance, in Fig. 20 we show the residual histograms for all modeling in the GGM EIGEN6C4.

Observing the histograms for the central zone, this one has the worst behavior of the three. Bias in the histogram can be appreciated caused undoubtedly by the heterogeneity of the orthometric heights, which not be absorbed by the model. Therefore, it is necessary to make densification and update the SRV in Santiago to obtain a more exhaustive analysis. Over this zone, we currently are

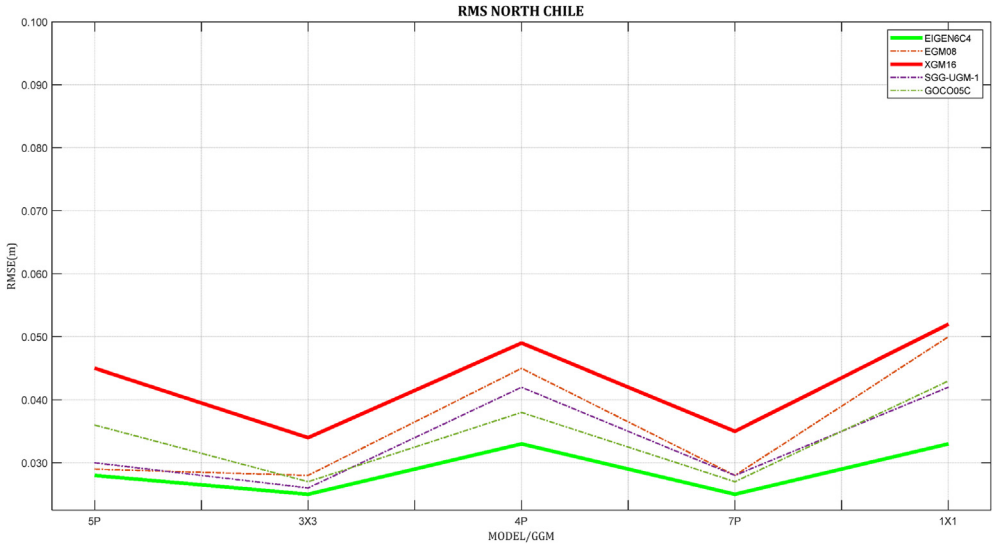

Fig. 14. RMSE by model and GGM in the northern zone of Chile.

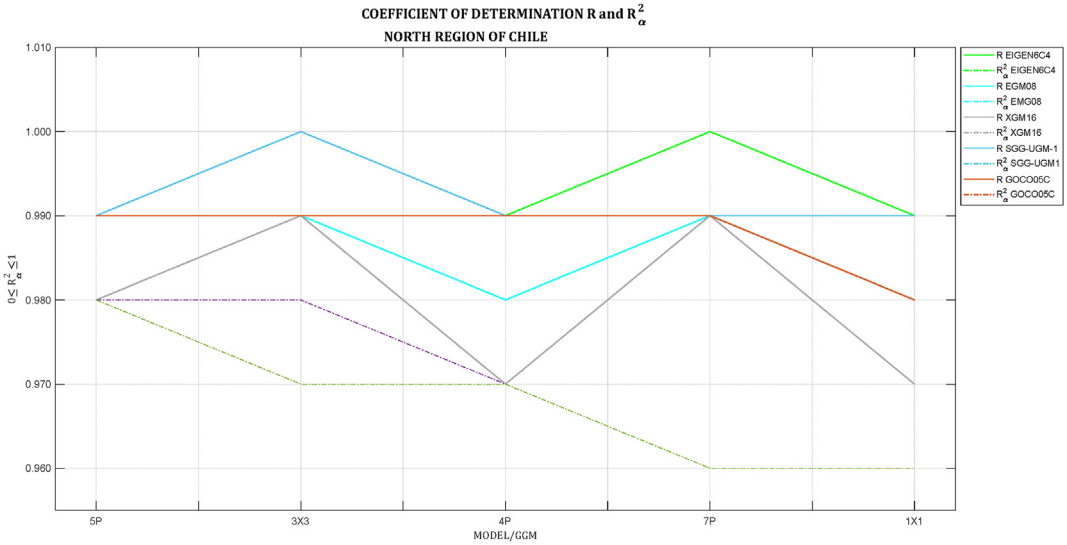

Fig. 15. Coefficient of determination of adjustment, northern zone of Chile, by model and GGM.

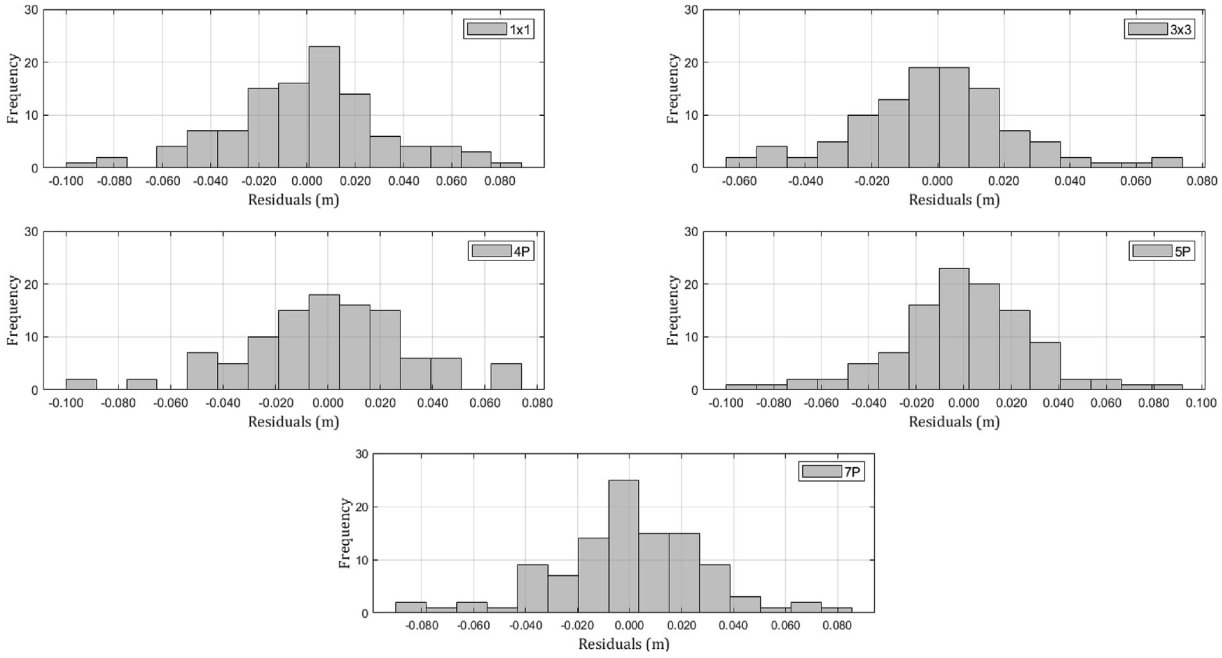

Fig. 16. Northern zone residuals histograms.

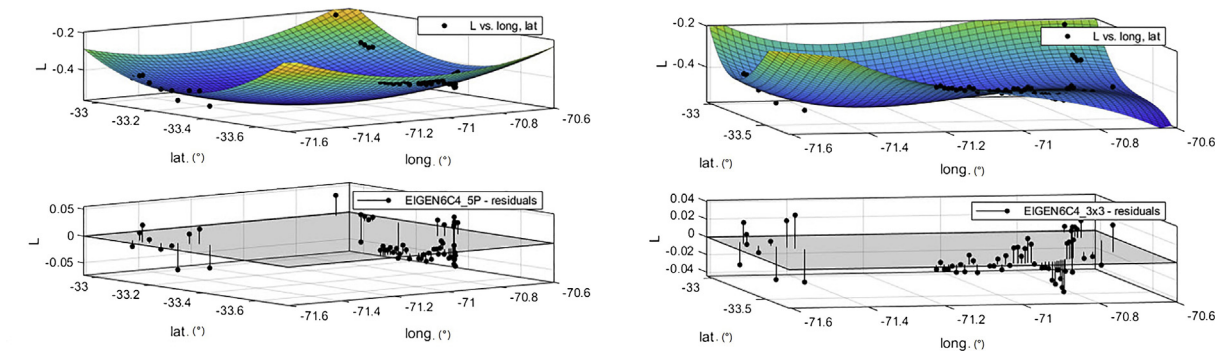

Fig. 17. 5P and 3 × 3 models on GGM EIGEN-6C4 central zone.

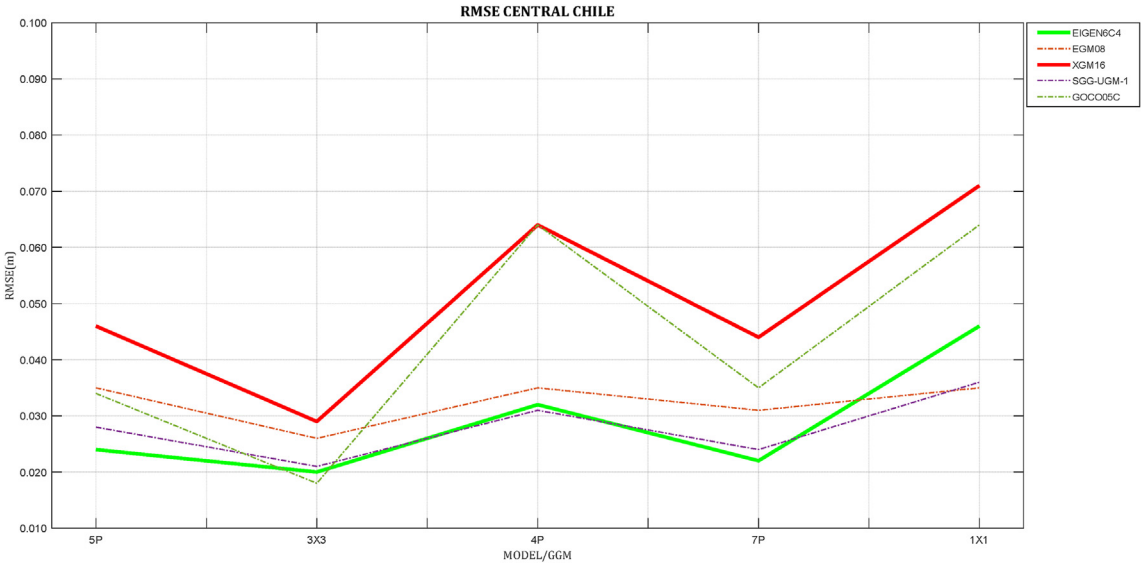

Fig. 18. RMS by model and GGM in the central zone of Chile.

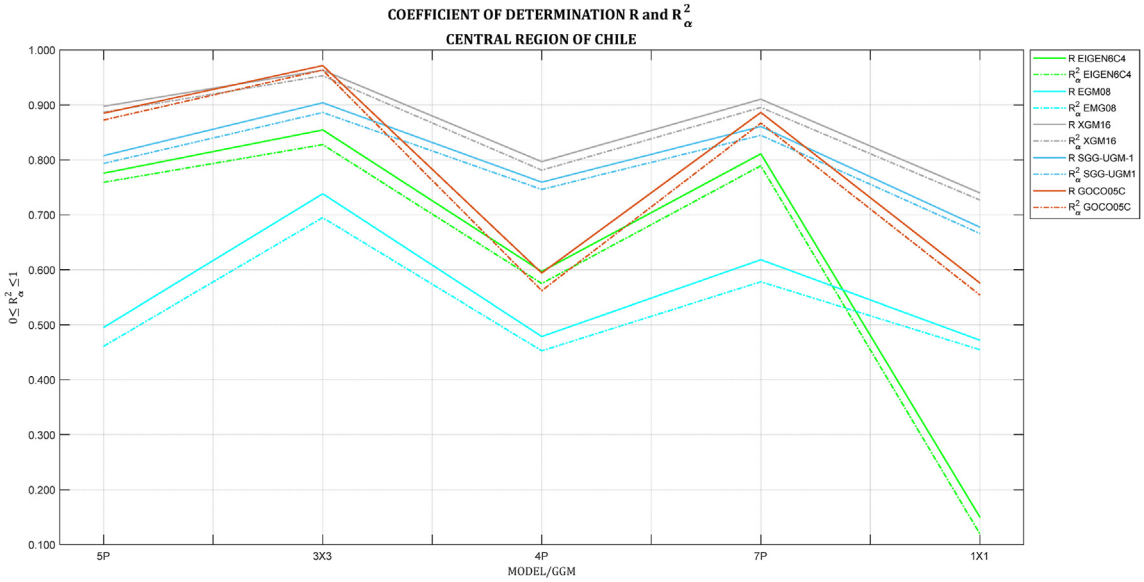

Fig. 19. Coefficient of determination of adjustment by model and GGM for the central zone of Chile.

doing observations of gravity to produce the same analysis, but with normal heights.

4.2. Spain modeling

The initial adjustment begins with 111 starting points, reduced to 107 points once 3 points are eliminated because of orthometric height wrongly registered in the monographs of the IGN, which generated a 3 m mistake. Application of the models shown in Section 2 generates surfaces such as those shown in Fig. 21.

The results of the correcting surface in the north of Spain are shown in Table 12 and graphs in Figs. 22 and 23.

In the north of Spain, the best GGM is again EIGEN-6C4, followed by EGM08 and SGG-UGM-1. The 3 × 3 polynomial has accuracies between 2.5 and 3 cm in almost all GMMs. Also, in Spain's case, the GGMs GOCO05C and XGM16 present a behavior substantially worse than in Chile, because the data from GOCO05C and XGM16 are independent of EGM08 [12].

Due to its better performance, in Fig. 24 we show the residual histograms for all modeling in the GGM EIGEN6C4.

By observing histograms in the north of Spain, we can see a better distribution of errors, along with a lower RMS than in the north of Chile and obviously lower than the central zone, closer to the seismic event of February 27. The previous observations undoubtedly show the problem of implanting IHRS

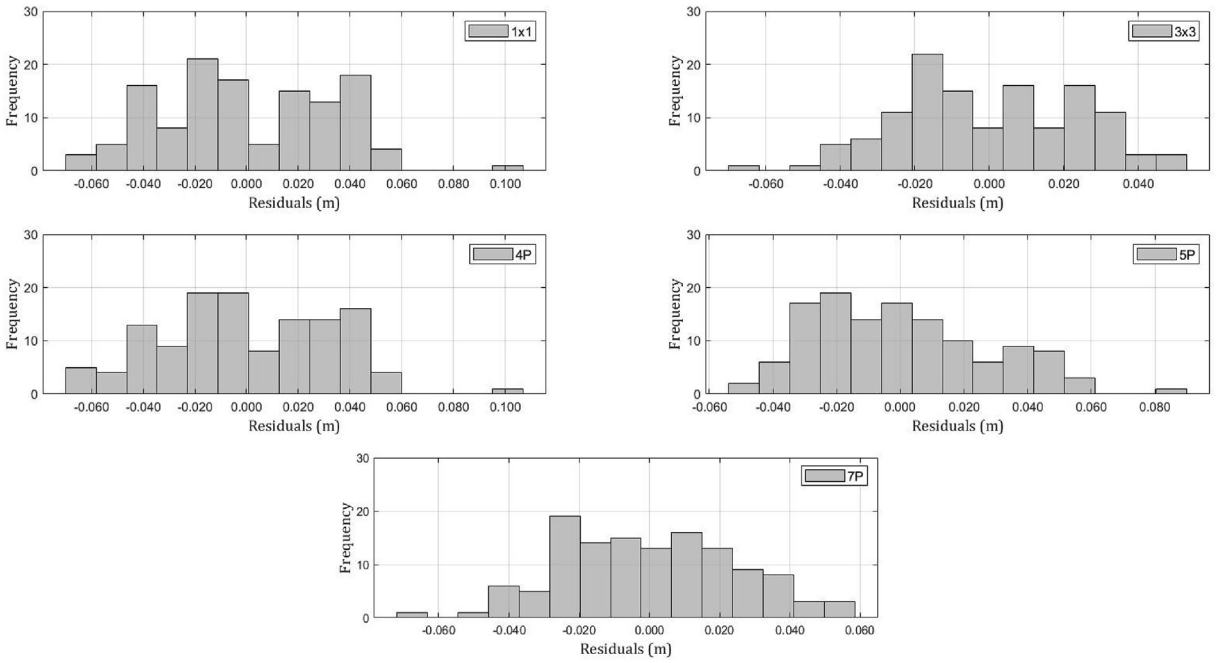

Fig. 20. Central zone residuals histograms.

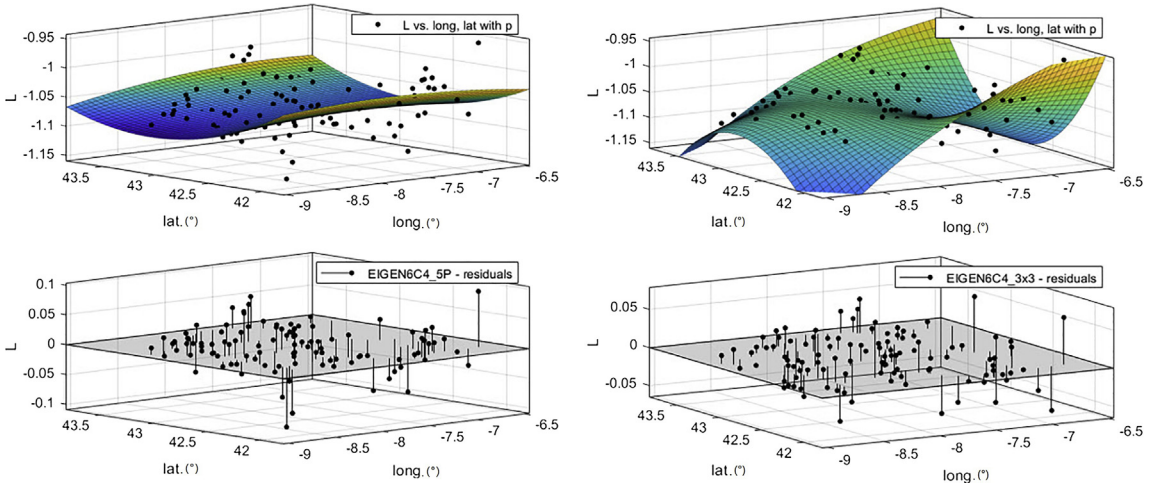

Fig. 21. 5P and 3 × 3 models on GGM EIGEN-6C4 in Spain.

on active seismic continents and with less dense and updated VRS.

4.3. Cross-validation

From this point, we proceed to perform the cross-validation explained in Section 2.3, by using the equation:

$$H = h - N - \boldsymbol{a}^{\mathbf{T}}\widehat{\boldsymbol{x}} \tag{3.1}$$

The 1 × 1 model represents a plane exclusively, and the 3 × 3 model does not represent the reference surface truthfully. Thus, for validation, we only use similar models of 4, 5, and 7 parameters for all GGMs, which are shown in Table 13.

For the 5P model, which is the best adjustment, cross-validation shows a deviation of 31 mm, 33 mm, and 35 mm in the zones of Spain and north and central Chile, respectively in Figs. 25–27.

The 5P model has similar behavior in the three zones for GGMs EIGEN-6C4 and EGM08. This model predicts the position of H with practically the same nominal precision of the GGM. However, it is now adapted to the VRS of each of the countries, which was not previously the case. The complete lack of terrestrial gravity data makes GGM SGG-UGM-1, GOCO05C, and XGM2016 have lower precision, with all of the cases between 4 and 5 cm, as shown in Table 3.

Analyzing SGG-UGM-1, GOCO05C, and XGM2016, we cannot indicate which is better than the other, because their behavior is nearly identical; there is only a slight upgrade of the SGG-UGM-1 in the northern zone of Spain and the central zone of Chile. However, this does not achieve the objective of using a hybrid model with

Table 12
Surface adjustments statistics on the northern region of Spain.

	SSE	R-Square	ADJ R-Square	RMSE(m)
EIGEN6C4				
5P	0.0979	0.2002	0.1688	0.031
3 × 3	0.0644	0.4737	0.4248	0.026
4P	0.1072	0.1241	0.0986	0.032
7P	0.0929	0.2414	0.1958	0.030
1 × 1	0.1137	0.0715	0.0536	0.033
EGM08				
5P	0.1236	0.3383	0.3124	0.035
3 × 3	0.0618	0.6691	0.6384	0.025
4P	0.1326	0.2900	0.2693	0.036
7P	0.1147	0.3860	0.3491	0.034
1 × 1	0.1343	0.2808	0.2670	0.036
SGG-UGM-1				
5P	0.1146	0.5483	0.5306	0.034
3 × 3	0.0618	0.7563	0.7337	0.025
4P	0.1508	0.4057	0.3883	0.038
7P	0.1032	0.5935	0.5691	0.032
1 × 1	0.1748	0.3113	0.2980	0.041
GOCO 05C				
5P	0.7308	0.3289	0.3026	0.085
3 × 3	0.5815	0.4660	0.4164	0.077
4P	0.8024	0.2632	0.2417	0.088
7P	0.7166	0.3420	0.3025	0.085
1 × 1	0.8661	0.2047	0.1894	0.091
XGM16				
5P	0.7167	0.2036	0.1724	0.084
3 × 3	0.6044	0.3283	0.2660	0.079
4P	0.7411	0.1764	0.1525	0.085
7P	0.7017	0.2202	0.1734	0.084
1 × 1	0.7564	0.1595	0.1433	0.085

enough precision for this GGMs, adapting the VRS to we can access directly with GNSS observations.

If we make a regional analysis in Chile, the cross-validation shows that the north region's hybrid model is more precise than the one in the central region, undoubtedly explained by the leveling data that come from H.

4.4. Results

Based on the previous discussion, we chose to use the combination EIGEN-6C4-5P model for the three zones of studies as the one with the best fit. This synergy allows accessing the VRS of each of the countries using the h heights from the GNSS receivers combined with GGM-H, all with cm accuracy. The results are three grids of the hybrid geoid (correction surface) that allow us to obtain orthometric heights with an average precision of around 3.5 cm. The archive structure is a ASCII grid file in each zone with values of:

$$\mathrm{ID} \quad \phi \quad \lambda \quad \mathrm{N(adapted)}$$

This file can be perfectly loadable in any geomatics program or GPS device. The Figs. 28–33 illustrate this characteristic.

5. Conclusions

In this research, we have shown satisfactorily how the modeling of corrective surfaces can be a good alternative for the compatibility of geometric GNSS data, with physical data from GGMs and the SRVs of each country, using what is known as “hybrid geoids” or “geometric geoids.” Of the large number of GGMs available in ICGEM, EIGEN6C4 and EGM080 are the ones that produced the best results, followed far behind by the other models tested. It became clear in this study that the 5P model, together with the EIGEN6C4 data, can be used continuously with more than enough precision for engineering, surveying, and cadastre work, both in northern Spain and in the two studied areas of Chile.

In Spain, even prior to extending the study to the entire country, the models (5P) and GGM(EIGEN6C4) have the best fit to generate a hybrid model for all of Spain. Having only one definition point for the SRV is an advantage for the study's continuity, of course. Unfortunately, this statement cannot be extrapolated to Chile because the other tide gauges' leveling lines have not been studied. It is worth mentioning here that as Chile's central region was observed, some outdated leveling data degraded the final results greatly. Still, in the meantime, because the IHRF is not fully operational, these leveling lines can be remeasured to improve the corrected surface.

In countries like Spain, the implementation of SRVs on a continental scale is, like the EVRS, more advanced than in developing countries, like Chile. Here the implementation of IHRS is still in a

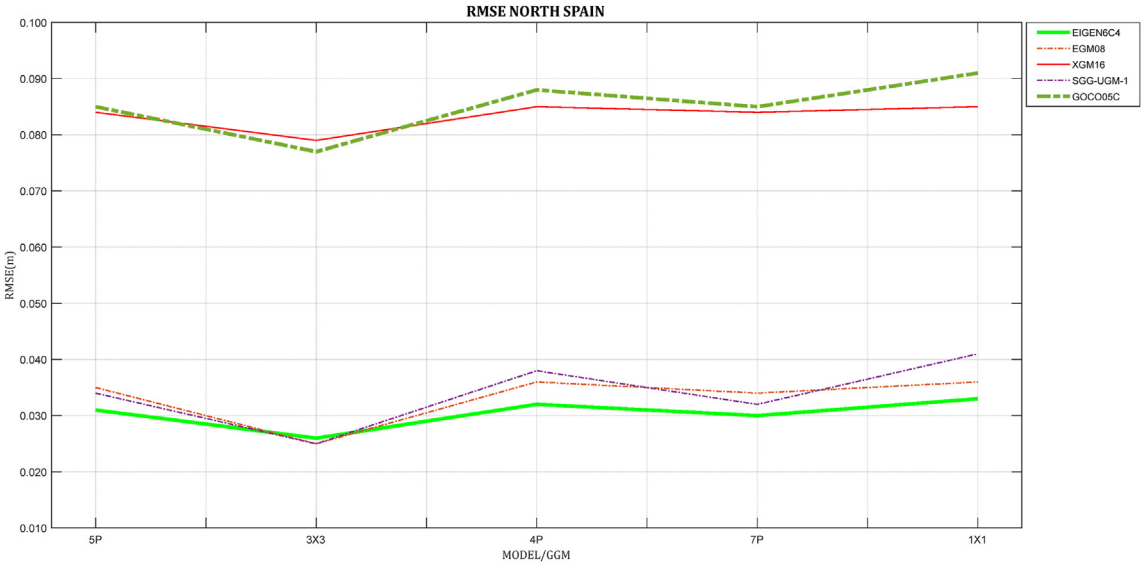

Fig. 22. RMSE and GGM by model in north of Spain.

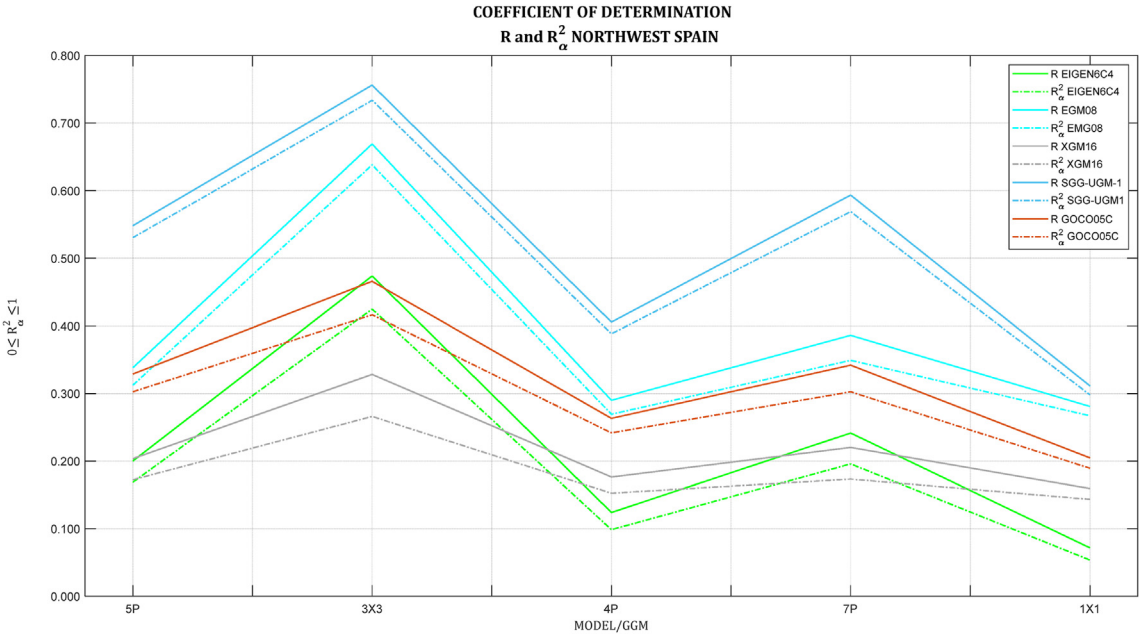

Fig. 23. Coefficient of determination of adjustment, north zone of Spain, by model and GGM.

study phase, and where also, a seismic event would make that a significant portion of the previous leveling and gravity campaign work must be done again. The awaited arrival of EGM2020, which will undoubtedly be deployed hand-in-hand with IHRF, will allow access to physical heights with greater precision than their predecessors. However, the accuracy linked to degree and order of this GGM will go in hand with the quantity of observed data in the field.

Although it is true it is the subject of another study but we used in this one, we can indicate that the EUREF velocity models satisfactorily fulfill their epoch-changing function. However, in South America, we see that modeling the height component in the existing models is not included (VEMOS). Furthermore, the few models that exist have generated inconsistencies in the residuals that the model cannot absorb. This second part is undoubtedly a new challenge in which we are working side by side with IGM of Chile and SIRGAS.

The start of work related to the implementation and use of IHRF in many countries has already begun. In others, IHRF stations

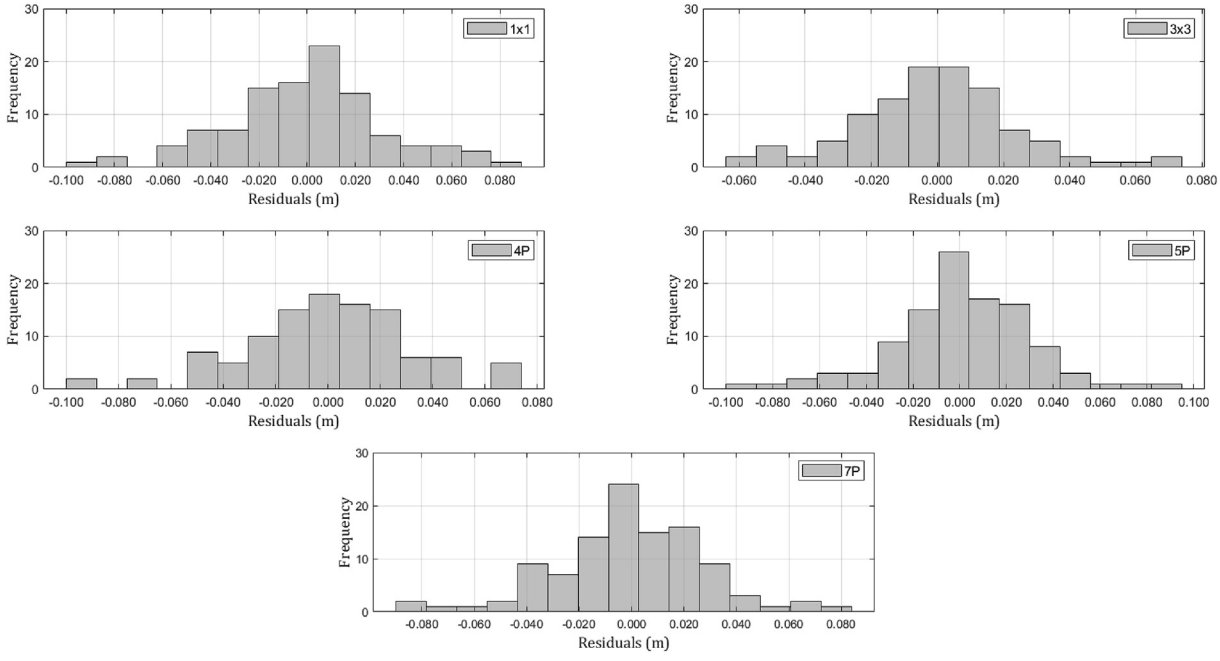

Fig. 24. North zone of Spain residuals histograms.

Table 13
Cross-validation of north, central Chile, and north of Spain.

NORTH REGION				CENTRAL REGION	
Model	GGM	Mean(m)	RMS(m)	Mean(m)	RMS(m)
4P	EIGEN6C4	0.000	0.036	0.004	0.038
	EGM08	0.000	0.035	0.002	0.040
	SGG-UGM-1	0.000	0.039	0.000	0.049
	GOCO05C	0.000	0.039	−0.008	0.050
	XGM2016	0.000	0.040	0.010	0.048
5P	EIGEN6C4	0.000	0.033	0.003	0.035
	EGM08	0.000	0.035	0.002	0.039
	SGG-UGM-1	0.000	0.042	0.001	0.046
	GOCO05C	0.000	0.041	−0.005	0.049
	XGM2016	0.000	0.043	0.008	0.048
7P	EIGEN6C4	−0.029	0.036	−0.004	0.038
	EGM08	−0.085	0.036	0.007	0.039
	SGG-UGM-1	−0.045	0.039	0.000	0.040
	GOCO05C	0.017	0.039	0.005	0.042
	XGM2016	0.000	0.040	0.028	0.040

NORTH SPAIN			
Model	GGM	Mean(m)	RMS(m)
4P	EIGEN6C4	0.000	0.036
	EGM08	0.000	0.037
	SGG-UGM-1	0.000	0.049
	GOCO05C	0.000	0.052
	XGM2016	0.000	0.051
5P	EIGEN6C4	0.000	0.034
	EGM08	0.000	0.035
	SGG-UGM-1	0.000	0.049
	GOCO05C	0.000	0.052
	XGM2016	0.000	0.051
7P	EIGEN6C4	−0.005	0.037
	EGM08	−0.007	0.038
	SGG-UGM-1	0.000	0.049
	GOCO05C	0.001	0.050
	XGM2016	0.001	0.048

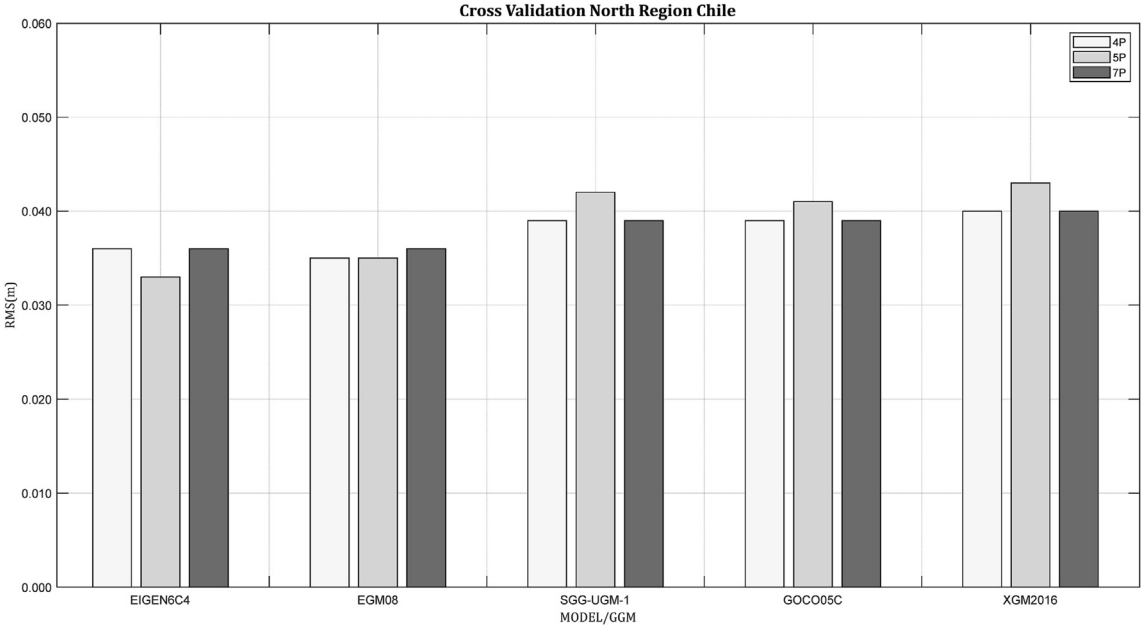

Fig. 25. Cross-validation north of Chile.

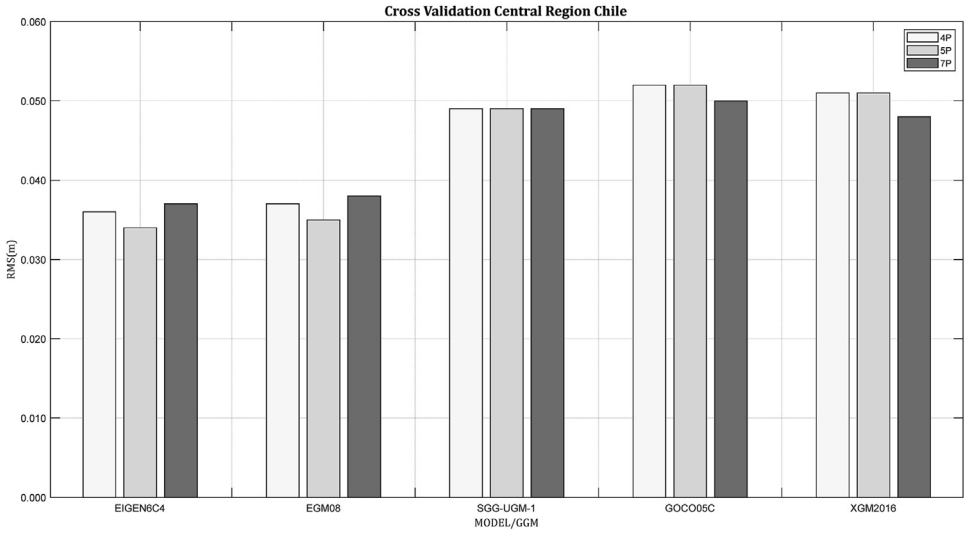

Fig. 26. Cross-validation central zone of Chile.

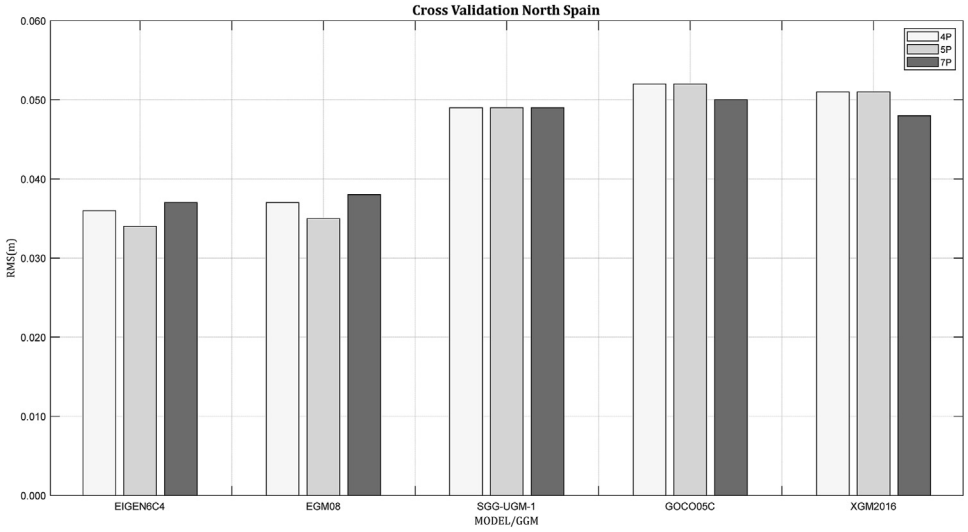

Fig. 27. Cross-validation north zone of Spain.

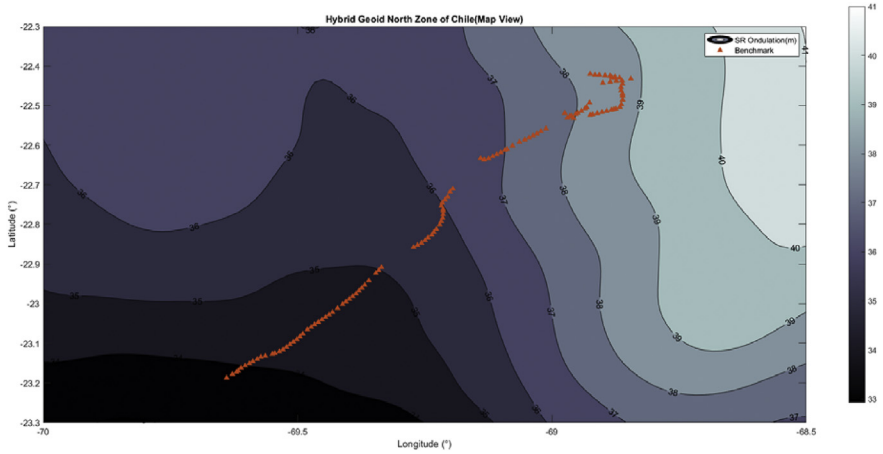

Fig. 28. Hybrid geoid grid for the north zone of Chile, map view.

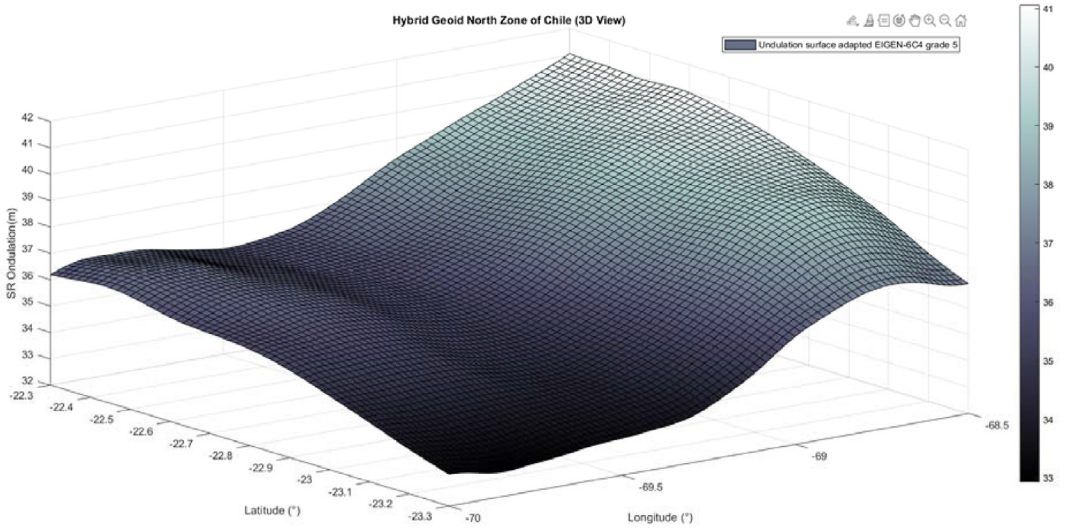

Fig. 29. Hybrid geoid grid for the north zone of Chile, 3D view.

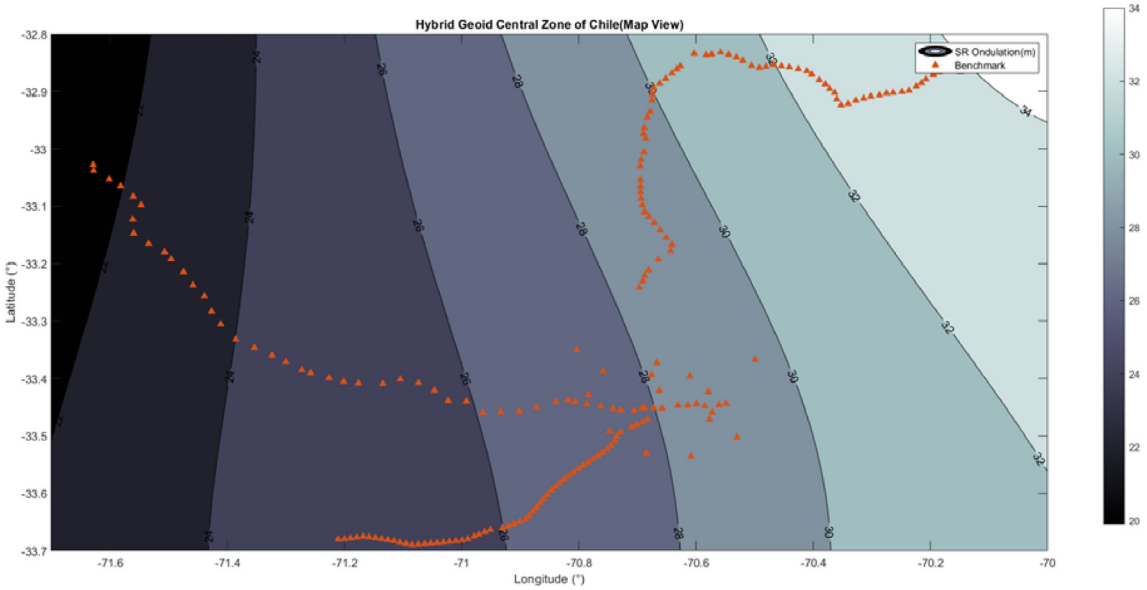

Fig. 30. Hybrid geoid grid for the central zone of Chile, map view.

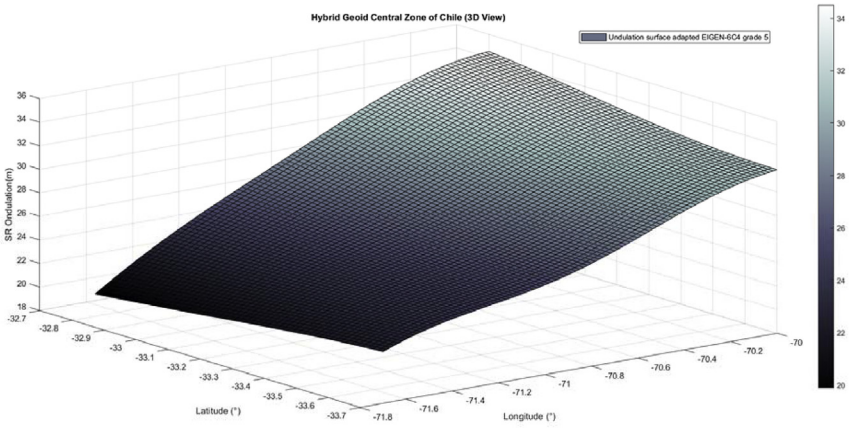

Fig. 31. Hybrid geoid grid for the central zone of Chile, 3D view.

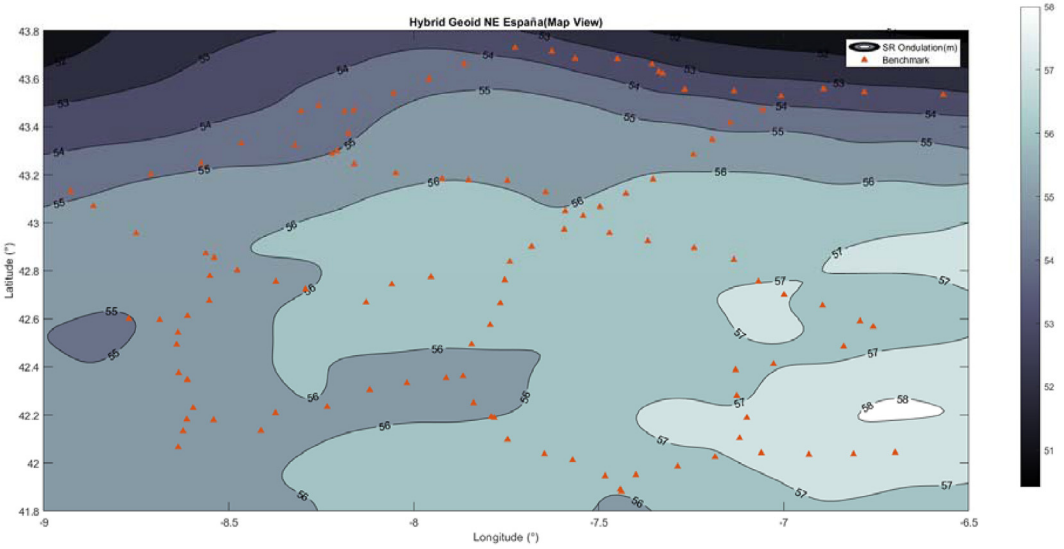

Fig. 32. Hybrid geoid grid for the north zone of Spain, map view.

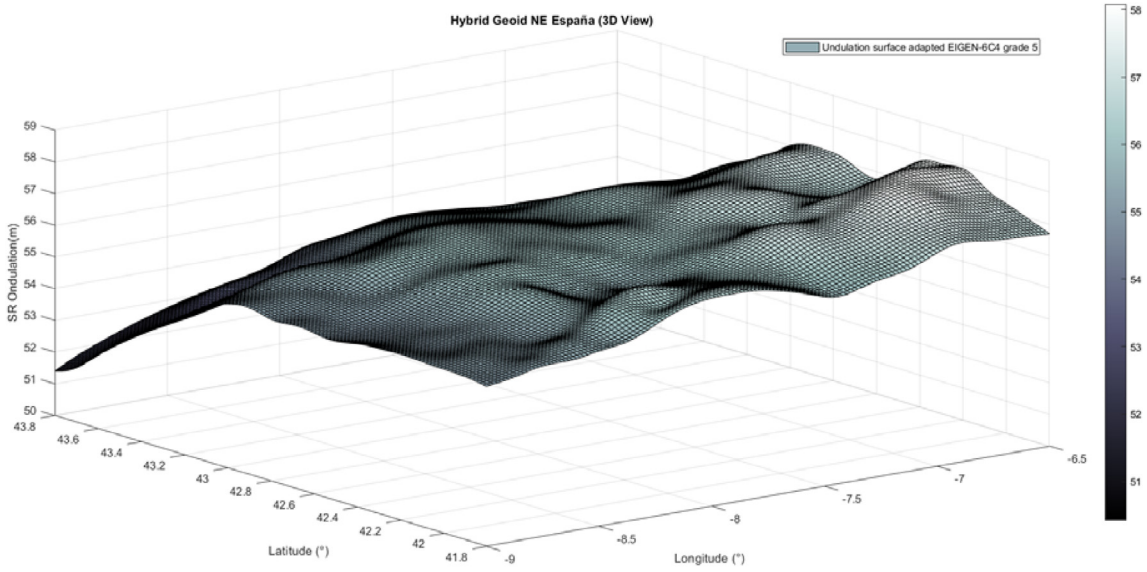

Fig. 33. Hybrid geoid grid for the north zone of Spain, 3D view.

do not exist, nor are they expected in the medium and short term. In addition to geopolitical reasons, another reason is financial: on the one hand, countries do not want to share geophysical data linked to natural resources, and on the other, leveling campaigns are long and expensive. If the possibility of a seismic event in countries like Chile is added to this, the maintenance of altimetric networks with field observations is increasingly complex. An earthquake or seismic event makes the work merely a snapshot of the moment, thus losing the 4d component until a new measurement is made. This article offers a vision and numerical analysis to model a hybrid geoid by combining the different heights that use the geodesy. This produces a reliable, precise, and above all, continuous tool to access the VRS in countries with fewer resources, more efficiently and robustly, until they have access to the IHRF.

Conflicts of interest

The authors declare that there is no conflicts of interest.

Acknowledgements

The authors wish to thank the Military Geographical Institute of Chile and National Geographic Institute of Spain for lending altimetry data, as well as to thank our classmates who have densified the VRS in both countries. Thanks to Trimble for providing the commercial license of the TBC v.4.0 software. The Matlab license code used is 40877188. The maps in the document were made with QGIS v3.09 [61]. The main author is grateful for financial support for the Chilean part of the project from the Scientific and

Technological Research Department of USACH (DICYT in Spanish) through the project DICYT-Regular O91612TM.

References

[1] L. Sánchez, R. Čunderlík, N. Dayoub, K. Mikula, Z. Minarechová, Z. Šíma, V. Vatrt, M. Vojtíšková, A conventional value for the geoid reference potential W0, J. Geodyn. 90 (2016) 815–835, https://doi.org/10.1007/s00190-016-0913-x.

[2] Heiskanen Moritz, Physical Geodesy : San Francisco W. H. Freeman and Company : Free Download, Borrow, and Streaming : Internet Archive, 1967. https://archive.org/details/HeiskanenMoritz1967PhysicalGeodesy/page/n21. (Accessed 3 May 2019).

[3] C. Kotsakis, M.G. Sideris, On the adjustment of combined GPS/levelling/geoid networks, J. Geodyn. 73 (1999) 412–421, https://doi.org/10.1007/s001900050261.

[4] Intergovernmental committee on surveying and mapping, Australian vertical working surface (AVWS), Intergov. Comm. Surv. Mapp. (2019). https://icsm.gov.au/sites/default/files/2019-12/AVWS Technical Implementation Plan_V1.0.pdf.

[5] D. Bolkas, G. Fotopoulos, M.G. Sideris, Referencing regional geoid-based vertical datums to national tide gauge networks, J. Geod. Sci. 2 (2013), https://doi.org/10.2478/v10156-011-0050-7.

[6] A. Kiliçoğlu, A. Direnç, H. Yildiz, M. Bölme, B. Aktuğ, M. Simav, O. Lenk, Regional gravimetric quasi-geoid model and transformation surface to national height system for Turkey (THG-09), Studia Geophys. Geod. (2011), https://doi.org/10.1007/s11200-010-9023-z.

[7] D. Arana, P.O. Camargo, G.N. Guimarães, Hybrid geoid model: theory and application in Brazil, An. Acad. Bras. Cienc. 89 (2017) 1943–1959, https://doi.org/10.1590/0001-3765201720160802.

[8] L. Sánchez, Kinematics of the SIRGAS reference frame, in: S. Sirgas (Ed.), Symp. SIRGAS2017, Mendoza, Argentina, 2017.

[9] E.S. Ince, F. Barthelmes, S. Reißland, K. Elger, C. Förste, F. Flechtner, H. Schuh, ICGEM – 15 years of successful collection and distribution of global gravitational models, associated services, and future plans, Earth Syst. Sci. Data 11 (2019) 647–674, https://doi.org/10.5194/essd-11-647-2019.

[10] N.K. Pavlis, S.a. Holmes, S.C. Kenyon, J.K. Factor, An Earth Gravitational Model to Degree 2160: EGM2008, 2008, Gen. Assem. Eur. Geosci. Union, Vienna, Austria, 2008. April 13-18.

[11] C. Förste, S. Bruinsma, O. Abrikosov, F. Flechtner, J. Marty, J.-M. Lemoine, C. Dahle, H. Neumayer, F. Barthelmes, R. König, R. Biancale, C. Förste, S. Bruinsma, O. Abrikosov, F. Flechtner, J. Marty, EIGEN-6C4 - the latest combined global gravity field model including GOCE data up to degree and order 2190 of GFZ Potsdam and GRGS Toulouse, EGU Gen. Assem. (2014), https://doi.org/10.5880/icgem.2015.1.

[12] T. Fecher, R. Pail, T. Gruber, GOCO05c: a new combined gravity field model based on full normal equations and regionally varying weighting, Surv. Geophys. 38 (2017) 571–590, https://doi.org/10.1007/s10712-016-9406-y.

[13] G. Font, M.C. Pacino, D. Blitzkow, C. Tocho, A preliminary geoid model for Argentina, in: Geod. Move, 2011, pp. 255–261, https://doi.org/10.1007/978-3-642-72245-5_37.

[14] D.A. Pinon, Development of a Precise Gravimetric Geoid Model for Argentina, 2016, p. 182, contains,Development of a Precise Gravime (accessed January 1, 2020), https://researchrepository.rmit.edu.au/discovery/fulldisplay?docid=alma9921864076501341&context=L&vid=61RMIT_INST:ResearchRepository&lang=en&search_scope=Research&adaptor=Local Search Engine&tab=Research&query=any.

[15] A.C.O. Cancoro de Matos, D. Blitzkow, Evaluation of recent GOCE geopotential models in South America, Newton's Bull. 5 (2015) 83, https://doi.org/10.2478/v10156-011-0033-8.

[16] J.A. Tarrío, Evaluación del Modelo Global de Geopotencial EIGEN-6C4 mediante GNSS/Nivelación en la Región Metropolitana de Chile, in: S. Sirgas (Ed.), Symp. SIRGAS2017, Mendoza, Argentina, 2017, https://doi.org/10.13140/RG.2.2.18778.24009.

[17] I.G.N. Centro de Observaciones Geodésicas, EL NUEVO MODELO DE GEOIDE PARA ESPAÑA EGM08 - REDNAP, 2007, pp. 1–21.

[18] J.A. Tarrío Mosquera, Resumen de tesis. Contraste de geoides gravimétricos con observaciones de nivelación geométrica y GPS en la comunidad de Galicia, 2014. http://hdl.handle.net/10366/125963. (Accessed 5 October 2019).

[19] V. Corchete, The high-resolution gravimetric geoid of North Iberia: NIBGEO, Terra. Nova 20 (2008) 489–493, https://doi.org/10.1111/j.1365-3121.2008.00844.x.

[20] Z. Altamimi, P. Rebischung, L. Métivier, X. Collilieux, ITRF2014: a new release of the International Terrestrial Reference Frame modeling nonlinear station motions, J. Geophys. Res. Solid Earth. 121 (2016) 6109–6131, https://doi.org/10.1002/2016JB013098.

[21] H. Drewes, Symposium SIRGAS 2017, in: S. Sirgas (Ed.), Varying Surf. Kinemat. Lat. Am., VEMOS 2009 , 2015, 2017, Mendoza, Argentina, 2017, pp. 27–29.

[22] C. Bruyninx, J. Legrand, A. Fabian, E. Pottiaux, GNSS metadata and data validation in the EUREF Permanent Network, GPS Solut. 23 (2019), https://doi.org/10.1007/s10291-019-0880-9.

[23] M. Bevis, A. Brown, Trajectory models and reference frames for crustal motion geodesy, J. Geodyn. 88 (2014) 283–311, https://doi.org/10.1007/s00190-013-0685-5.

[24] J.A. Tarrío Mosquera, G. Lira, P. Cepeda, Evaluación del movimiento del marco de referencia terrestre con técnicas GNSS, en zonas de riesgo sísmico, Universidad de Santiago de Chile, 2018.

[25] J.A. Tarrío Mosquera, Webinar, Datos y herramientas GNSS de acceso libre, Youtube, 2020. https://youtu.be/QuhuBKCmnFc. (Accessed 1 September 2020).

[26] P.F. Rolf Dach, Simon Lutz, Peter Walser, Bernese GNSS Software, Version 5.2, User Manual, vol. 47, Astron. Institute, Univ. Bern, Bern Open Publ, 2015, p. 884, https://doi.org/10.7892/boris.72297.

[27] Servicio Nacional de Geología y Minería, ESTUDIO DE PREFACTIBILIDAD DE DATÚM GEODÉSICO DE LAS CONCESIONES MINERAS, Merc. Publico, 2019, in: https://www.mercadopublico.cl/Procurement/Modules/RFB/DetailsAcquisition.aspx?qs=+DstyBefjDuACMPaG66S0Q==. (Accessed 1 September 2020).

[28] EUREF WG on European Dense Velocities, European dense velocities, Fed. Off. Topogr. Swisstopo. (2016). http://pnac.swisstopo.admin.ch/divers/dens_vel/index.html. (Accessed 9 January 2020).

[29] H.D. Montecino, S.R.C. de Freitas, J.C. Báez, V.G. Ferreira, Effects on Chilean vertical reference frame due to the Maule earthquake co-seismic and post-seismic effects, J. Geodyn. 112 (2017) 22–30, https://doi.org/10.1016/j.jog.2017.07.006.

[30] M. Ekman, Impacts of geodynamic phenomena on systems for height and gravity, Bull. Geod. 63 (1989) 281–296, https://doi.org/10.1007/BF02520477.

[31] Y.C. Li, M.G. Sideris, Minimization and estimation of geoid undulation errors, Bull. Geod. 68 (1994) 201–219, https://doi.org/10.1007/BF00808101.

[32] Y.Q. Chen, Z. Luo, A hybrid method to determine a local geoid model - case study, Earth, Planets Sp. 56 (2004) 419–427, https://doi.org/10.1186/BF03352495.

[33] G. Fotopoulos, An Analysis on the Optimal Combination of Geoid , Orthometric and Ellipsoidal Height Data, Dep. Geomatics Eng. Univ. Calgary., 2003, p. 230. http://www.geomatics.ucalgary.ca/links/GradTheses.html.

[34] F. Sansò, M. Sideris, Geoid Determination, 2013. http://link.springer.com/content/pdf/10.1007/978-3-540-74700-0.pdf.

[35] B.B. Frey, Gauss–markov theorem, in: SAGE Encycl. Educ. Res. Meas. Eval, SAGE Publications, Inc., 2018, https://doi.org/10.4135/9781506326139.n282.

[36] G. Fotopoulos, Calibration of geoid error models via a combined adjustment of ellipsoidal, orthometric and gravimetric geoid height data, J. Geodyn. (2005), https://doi.org/10.1007/s00190-005-0449-y.

[37] F.G. Lemoine, D.E. Smith, L. Kunz, R. Smith, E.C. Pavlis, N.K. Pavlis, S.M. Klosko, D.S. Chinn, M.H. Torrence, R.G. Williamson, C.M. Cox, K.E. Rachlin, Y.M. Wang, S.C. Kenyon, R. Salman, R. Trimmer, R.H. Rapp, R.S. Nerem, The development of the joint NASA GSFC and the national imagery and mapping agency (NIMA) geopotential model EGM96, gravity, Geoid Mar. Geod. (1997) 461–469, https://doi.org/10.1007/978-3-662-03482-8_62.

[38] J. Ihde, W. Augath, The European vertical reference system (EVRS), in: Its relation to a world height system and to the ITRS, 2002, https://doi.org/10.1007/978-3-662-04709-5_14.

[39] L. Sanchez, Definition and realisation of the SIRGAS vertical reference system within a globally unified height system, in: Int. Assoc. Geod. Symp., 2007, pp. 638–645, https://doi.org/10.1007/978-3-540-49350-1_92.

[40] A.G. Santacruz Jaramillo, Desarrollo de estrategias para integración de las Redes Verticales de América del Sur con base en los términos de referencia SIRGAS/GGOS/IAG, Rev. Cartogr. (2019), https://doi.org/10.35424/rcar.v0i96.187.

[41] J. Ihde, R. Barzaghi, U. Marti, L. Sánchez, M. Sideris, H. Drewes, C. Foerste, T. Gruber, G. Liebsch, R. Pail, Report of the ad-hoc group on an international height reference system (IHRS), Trav. l'AIG. 39 (2015) 2011–2015.

[42] Sirgas, Sistema de Referencia Geocéntrico para las Américas, 2019, 2019. www.sirgas.org. (Accessed 29 April 2019).

[43] R. Maturana, R. Barriga, The vertical geodetic network in Chile, in: Vert. Ref. Syst. Int. Assoc. Geod. Symp., 2013, pp. 23–26, https://doi.org/10.1007/978-3-662-04683-8_6.

[44] Commission Intergovernmental Oceanographic, Unesco, Sea level station monitoring facility (n.d.), http://www.ioc-sealevelmonitoring.org/list.php?operator=59&showall=a&output=performance#.

[45] Instituto Geográfico Nacional, Red de Nivelación de la República Argentina, 2017. http://ramsac.ign.gob.ar/posgar07_pg_web/documentos/Informe_Red_de_Nivelacion_de_la_Republica_Argentina.pdf.

[46] L. Sánchez, M.G. Sideris, Vertical datum unification for the international height reference system (IHRS), Geophys. J. Int. (2017) 570–586, https://doi.org/10.1093/gji/ggx025.

[47] W.E. Featherstone, M. Kuhn, Height systems and vertical datums: a review in the australian context, J. Spat. Sci. 51 (2006) 21–41, https://doi.org/10.1080/14498596.2006.9635062.

[48] N.J. Brown, J.C. McCubbine, W.E. Featherstone, N. Gowans, A. Woods, I. Baran, AUSGeoid2020 combined gravimetric–geometric model: location-specific uncertainties and baseline-length-dependent error decorrelation, J. Geodyn. 92 (2018) 1457–1465, https://doi.org/10.1007/s00190-018-1202-7.

[49] Instituto Geográfico Nacional de España, Teoria de Geodesia, 1984. http://www.ign.es/web/resources/docs/IGNCnig/GDS-Teoria-Geodesia.pdf.
[50] R. Rummel, G. Balmino, J. Johannessen, P. Visser, P. Woodworth, Dedicated gravity field missions - principles and aims, J. Geodyn. 33 (2002) 3–20, https://doi.org/10.1016/S0264-3707(01)00050-3.
[51] Franz Barthelmes, Definition of Functionals of the Geopotential and Their Calculation from Spherical Harmaonic Models, 2009, pp. 1–36, https://doi.org/10.2312/GFZ.b103-0902-26.
[52] N.K. Pavlis, S.A. Holmes, S.C. Kenyon, J.K. Factor, The development and evaluation of the Earth gravitational model 2008 (EGM2008), J. Geophys. Res. Solid Earth. 117 (2012), https://doi.org/10.1029/2011JB008916 n/a-n/a.
[53] W. Liang, SGG-UGM-1: The High Resolution Gravity Field Model Based on the EGM2008 Derived Gravity Anomalies and the SGG and SST Data of GOCE Satellite, GFZ Data Serv, 2018, https://doi.org/10.11947/j.AGCS.2018.20170269.
[54] E. Nicacio, R. Dalazoana, S. De Freitas, F.E. Method, S. Free, Evaluation of the ultra-high resolution global geopotential model SGG-UGM-1 in the Brazilian southern region evaluation of the ultra-high resolution global geopotential model SGG-UGM-1 in THE Brazilian, in: An. Do VII SIMGEOPublisher Ed. UFPE, RECIFE, 2018, pp. 609–618.
[55] J. Mäkinen, J. Ihde, The permanent tide in height systems, in: Int. Assoc. Geod. Symp, pringer, Berlin, Heidelberg, 2009, pp. 81–87, https://doi.org/10.1007/978-3-540-85426-5_10.
[56] R. Rummel, Height unification using GOCE, J. Geod. Sci. 2 (2013) 355–362, https://doi.org/10.2478/v10156-011-0047-2.
[57] J. Kostelecký, J. Klokočník, B. Bucha, A. Bezděk, C. Förste, Evaluation of gravity field model EIGEN-6C4 by means of various functions of gravity potential, and by GNSS/levelling, Geoinformatics FCE CTU, 2015, https://doi.org/10.1002/2014GL062045.
[58] Mathworks, Curve Fitting Toolbox: For Use with MATLAB®: User's Guide, 2017. http://publication/uuid/1AB1E427-49D2-43BA-BE5C-B64EE88F3947.
[59] C. Tocho, Evaluation of GOCE/GRACE derived global geopotential models over Argentina with collocated GPS/levelling observations, Int. Assoc. Geodes. Symp. 141 (2014) 2–4, https://doi.org/10.1007/978-3-319-10837-7.
[60] Dirección de Vialidad, Ministerio de Obras Públicas - Dirección de Vialidad, 2019. http://www.vialidad.cl/areasdevialidad/manualdecarreteras/Paginas/default.aspx. (Accessed 11 May 2020).
[61] QGIS Geographic Information System., QGIS Development Team, Open Source Geospatial Found. Proj. (2020), 2019. https://qgis.org/es/site/. (Accessed 1 January 2020).

José Antonio Tarrío Mosquera was born in Santiago de Compostela, Spain in 1980. He received the M.S. and Ph.D. degrees in geodesy and GNSS technologies from Salamanca University(Spain) in 2009 and 2014. Since 2015 he works as an academic researcher at the University of Santiago de Chile, in charge of the line of research in Geodesy and GNSS in the Geographical Engineering Department, teaching in Satellite Geodesy, Geodetic Adjustment, Geodesy and geomatics' applications with drones. Since 2017 He is the director of the USC geodetic analysis and processing center, associated with SIRGAS. At present Prof Dr. Tarrío is the Chair of SC 1.3b: South and Central America and chair of working group I in SIRGAS, currently belongs to IGS's Governing Board.

Marcelo Caverlotti Silva Doctor of Engineering Sciences, Degree in engineering sciences from University of Santiago of Chile (USACH), subdirector of the USC geodetic analysis and processing center, associated with SIRGAS.

Fernando Isla Surveyor technician, in charge of data management at the USC Processing Center.

Carlos Prado Master degree in Geoinformation Science and Earth Observation for Geoinformatics from the University or Twente. At the present he is the subdirector at the Geographic Military Institute of Chile